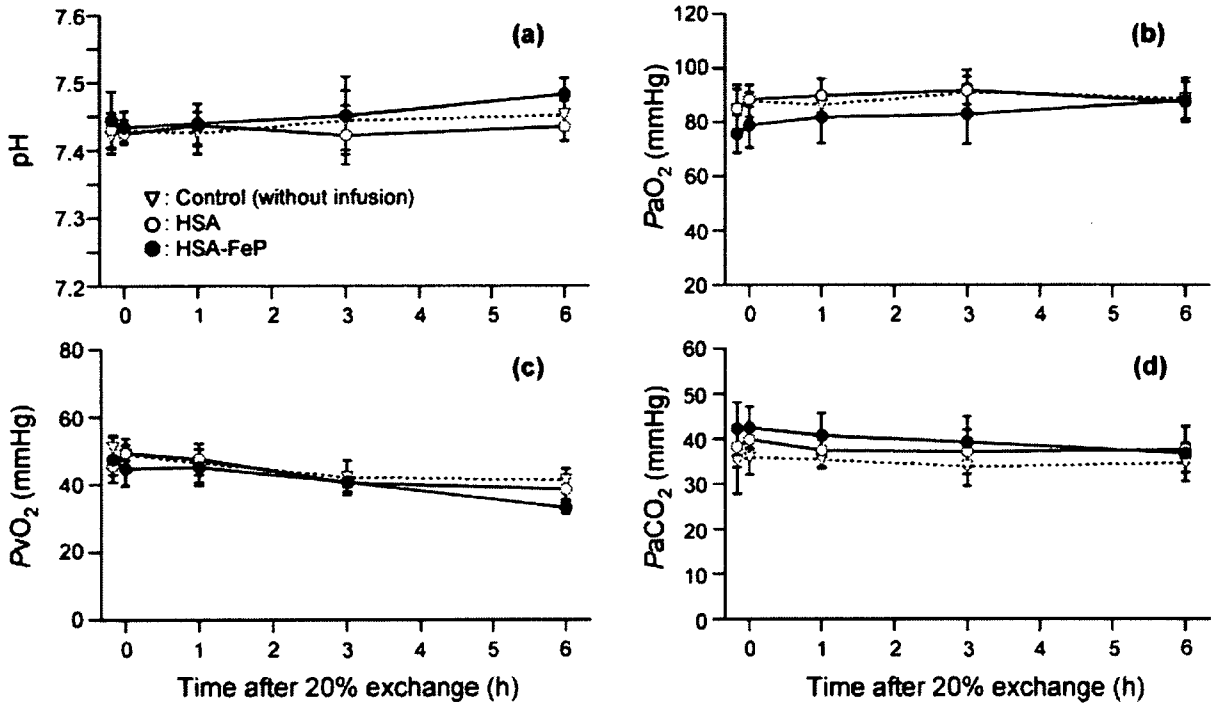

Figure 5. Time courses of (a) blood pH, (b) arterial blood O_2-pressure (PaO_2), (c) venous blood O_2-pressure (PvO_2), and (d) arterial blood CO_2-pressure ($PaCO_2$) in anesthetized rats after 20% exchange transfusion with HSA-FeP or HSA solution. Each value represents the mean ± SD ($n = 6$).

min-heme does not facilitate the immunological reaction and platelet activation in human blood at least based on the present test situation and degree.

Circulation parameters

After the 20% exchange transfusion with the HSA or HSA-FeP solution, Hct decreased ~80% of the basal values [Fig. 4(a)]. The body temperature of each group was maintained constant within 36.9–37.4°C during the experiments [Fig. 4(b)]. The time courses of MAP and HR of the HSA-FeP group were almost the same as those of the control or HSA group for 6 h [Fig. 4(c,d)]. Our previous studies showed that the infusion of HSA-FeP did not induce vasoconstriction and hypertension because of the low permeability of the albumin scaffold through the vascular endotheterlium.[20] It has been again demonstrated that absolutely no vasoactive response occurs after the 20% volume infusion of HSA-FeP.

Blood gas parameters

Changes in the blood gas parameters during the 20% exchange transfusion are shown in Figure 5(a–d). Differences in pH among the three groups were in the narrow range of 7.42–7.48 [Fig. 5(a)]. The PaO_2, PvO_2, and $PaCO_2$ values of the control, HSA, and HSA-FeP groups were also constant in the range of 78.9–91.8, 33.2–49.5, and 33.9–42.6 mmHg, respectively, by the end of the measurements [Fig. 5(b–d)]. These results revealed that HSA-FeP satisfies the initial preclinical safety as an RBC substitute.

In summary, one of the most prominent characteristics of the HSA-based O_2-carrier is its high blood compatibility, and no effect on the human immunological reaction and platelet activation. The appearance of the animals demonstrated no change for 6 h after the 20% exchange transfusion with HSA-FeP. The physiological responses in the HSA-FeP group were identical to those of the control and HSA groups. These results allow us to now undertake further advanced preclinical testing of this entirely synthetic O_2-carrier.

References

1. Chang TMS. Recent and future developments in modified hemoglobin and microencapsulated hemoglobin as red blood cell substitutes. Artif Cells Blood Substit Immobil Biotechnol 1997;25: 1–24.
2. Riess JG. Oxygen carriers ("blood substitute")—raison d'etre, chemistry, and some physiology. Chem Rev 2001;101:2797–2919.
3. Squires JE. Artificial blood. Science 2002;295:1002–1005.
4. Winslow R. Blood Substitutes. London: Elsevier; 2006.

5. Komatsu T, Hamamatsu K, Wu J, Tsuchida E. Physicochemical properties and O_2-coordination structure of human serum albumin incorporating tetrakis(*o*-pivamido)phenylporphyrinatoiron(II) derivatives. Bioconjug Chem 1999;10:82–86.
6. Tsuchida E, Komatsu T, Matsukawa Y, Hamamatsu K, Wu J. Human serum albumin incorporating tetrakis(*o*-pivalamido)-phenylporphinatoiron(II) derivative as a totally synthetic O_2-carrying hemoprotein. Bioconjug Chem 1999;10:797–802.
7. Komatsu T, Matsukawa Y, Tsuchida E. Effect of heme structure on O_2-binding properties of human serum albumin-heme hybrids: Intramolecular histidine coordination provides a stable O_2-adduct complex. Bioconjug Chem 2002;13:397–402.
8. Huang Y, Komatsu T, Nakagawa A, Tsuchida E, Kobayashi S. Compatibility in vitro of albumin-heme (O_2-carrier) with blood cell components. J Biomed Mater Res A 2003;66:292–297.
9. Hunag Y, Komatsu T, Yamamoto H, Horinouchi H, Kobayashi K, Tsuchida E. Exchange transfusion with entirely synthetic red-cell substitute albumin-heme into rats: Physiological responses and blood biochemical tests. J Biomed Mater Res A 2004;71:63–694.
10. Szebeni J, Wassef NM, Hartman KR, Alving CR. Complement activation in vitro by the red cell substitute, liposome-encapsulated hemoglobin: Mechanism of activation and inhibition by soluble complement receptor type 1. Transfusion 1997;37:150–159.
11. Shattil SJ, Hoxie A, Cunnington M, Brass LF. Changes in the platelet membrane glycoprotein IIb-IIIa complex during the platelet activation. J Biol Chem 1985;260:11107–11114.
12. Takagi J, Petre BM, Walz T, Springer TA. Global conformational rearrangements in integrin extracellular domains in outside-in and inside-out signaling. Cell 2002;110:599–611.
13. Xiao T, Takagi J, Coller BS, Wang JH, Springer TA. Structural basis for allostery in integrins and binding to fibrinogen-mimetic therapeutics. Nature 2004;432:59–67.
14. Marguerie GA, Plow EF, Edgington TS. Human platelets possess an inducible and saturable receptor specific for fibrinogen. J Biol Chem 1979;254:5357–5363.
15. Lasky LA. Selectin: Interpreters of cell-specific carbohydrate information during inflammation. Science 1992;258:964–969.
16. Stenberg PE, McEver RP, Shuman MA, Jacques YV, Bainton DF. A platelet alpha-granule membrane protein (GMP-140) is expressed on the plasma membrane after activation. J Cell Biol 1985;101:800–886.
17. Wakamoto S, Fujihara M, Abe H, Yamaguchi M, Azuma H, Ikeda H, Takeoka S, Tsuchida E. Effects of hemoglobin vesicles on resting and agonist-stimulated human platelets in vitro. Artif Cells Blood Substit Biotechnol 2005;33:101–111.
18. Ohtani W, Nawa Y, Takeshima K, Kamuro H, Kobayashi K, Ohmura T. Physiochemical and immunochemical properties of recombinant human serum albumin from *Pichia pastoris*. Anal Biochem 1998;256:56–62.
19. Taub R, Gould RJ, Garsky VM, Ciccarone TM, Hoxie J, Friedman PA, Shattil SJ. A monoclonal antibody against the platelet fibrinogen receptor contains a sequence that mimics a receptor recognition domain receptor. J Biol Chem 1989;264:259–265.
20. Tsuchida E, Komatsu T, Matsukawa Y, Nakagawa A, Sakai H, Kobayashi K, Suematsu M. Human serum albumin incorporating synthetic heme: Red blood cell substitute without hypertension by nitric oxide scavenging. J Biomed Mater Res A 2003;64:257–261.

Induced Long-Range Attractive Potentials of Human Serum Albumin by Ligand Binding

Takaaki Sato,[1,2,*] Teruyuki Komatsu,[2,3] Akito Nakagawa,[2] and Eishun Tsuchida[2,†]

[1]*Division of Pure and Applied Physics, Faculty of Science and Engineering, Waseda University, 3-4-1 Okubo, Shinjuku-ku, Tokyo 169-8555, Japan*

[2]*Advanced Research Institute for Science and Engineering, Waseda University, 3-4-1 Okubo, Shinjuku-ku, Tokyo 169-8555, Japan*

[3]*PRESTO, Japan Science and Technology Agency (JST), 4-1-8 Honcho, Kawaguchi-shi, Saitama 332-0012, Japan*

(Received 9 July 2006; published 15 May 2007)

Small-angle x-ray scattering and dielectric spectroscopy investigation on the solutions of recombinant human serum albumin and its heme hybrid revealed that heme incorporation induces a specific long-range attractive potential between protein molecules. This is evidenced by the enhanced forward intensity upon heme binding, despite no hindrance to rotatory Brownian motion, unbiased colloid osmotic pressure, and discontiguous nearest-neighbor distance, confirming monodispersity of the proteins. The heme-induced potential may play a trigger role in recognition of the ligand-filled human serum albumins in the circulatory system.

DOI: 10.1103/PhysRevLett.98.208101 PACS numbers: 87.14.Ee, 61.10.Eq, 83.80.Lz

Human serum albumin (HSA) is the most abundant plasma protein in our bloodstream, whose primary functions are transportation of hydrophobic molecules and adjustment of colloid osmotic pressure (COP) of blood [1]. Owing to its nonspecific ligand-binding capability, HSA has served many potential medical applications. Information on HSA-ligand interactions and their structural basis have recently been available by x-ray crystal structure analysis [2–5]. Such approaches have provided a structural foundation to create functional protein-ligand complexes. One of the promising materials is the rHSA-heme hybrid that can transport oxygen as hemoglobin does [6–9]. The material is currently investigated in preclinical tests as an artificial blood substitute [8]. Recent manifold interests in protein crystallography, critical phenomena, and disease processes have attracted increasing attention to interparticle interactions in globular protein solutions [10–15]. However, the fundamental problems like an influence of the ligand-binding upon protein-protein interactions remain elusive.

We investigated solutions of recombinant HSA (rHSA) (MW 66.5 kDa) and its heme hybrid [rHSA-heme; rHSA incorporating four iron-porphyrins (synthetic hemes)] [7]. Using small-angle x-ray scattering (SAXS), we scrutinized spatial correlations of these proteins in a 0.15M phosphate buffer saline (PBS) solution to fulfil ionic strength and pH close to physiological conditions and those in water to minimize ionic strength. The PBS solution of rHSA-heme (heme/rHSA = 4, mol/mol) was prepared according to our previously reported procedures [7]. The deionization of the protein sample was performed by several cycles of centrifugation/dilution with pure water using a Millipore Amicon Ultra to give aqueous solution of rHSA-heme. The solutions were passed through a 0.22 μm filter before all measurements. The deep red-colored, transparent solution of rHSA-heme can long be stored without precipitation or liquid-liquid phase separation. It has been confirmed that isoelectric point (pI), solution viscosity, and COP for rHSA-heme under the physiological environment are identical to those of rHSA.

All SAXS experiments were carried out by using a SAXSess camera (Anton Paar) in the q range of 0.072–5 nm^{-1}. A model-independent collimation-correction procedure was made via an indirect Fourier transformation (IFT) routine and/or based on a Lake algorithm. We also performed dielectric relaxation spectroscopy (DRS) experiments on aqueous rHSA and rHSA-heme solutions in the frequency range of $0.0005 \leq \nu/\mathrm{GHz} \leq 20$ using time domain reflectometry [16].

Figure 1 shows SAXS experiments on a concentration series of rHSA in PBS solution at 25 °C. The normalized scattered intensities $I(q)/c$, where $I(q)$ is the scattered intensity at scattering vector q and c the protein concentration, exhibit a decreasing forward intensity $I(q \rightarrow 0)/c$ with increasing c [Fig. 1(a)]. HSA carries a net negative charge of about 18 electronic charges at pH 7.4 [1]. Since the long-range electrostatic repulsion between rHSAs is efficiently screened in the PBS solutions, the suppressed forward intensity is mainly attributed to the decreased osmotic compressibility due to the increased particle number density. Lowering c results in the convergence of $I(q)/c$ to the intrinsic form factor $P(q)$ of rHSA, achieving the structure factor $S(q) \sim 1 (c \rightarrow 0)$.

The pair-distance distribution functions $p(r)$ of rHSA [Fig. 1(b)] in solution are obtained using generalized indirect Fourier transformation (GIFT) technique [17], for which we approximated $S(q)$ assuming a Yukawa potential and the Rogers-Young closure. The procedure confirms the existence of oblatelike particles having the maximum diameter of $D_{\max} \sim 8.0$–8.5 nm at all c. All features of $p(r)$ highly resemble those calculated from x-ray crystallography data on HSA (Protein Data Bank code 1UOR) [3].

Figure 2(a) presents variation of $I(q)$ of rHSA solutions, depending on the presence and absence of the heme incorporation and ionic strength of solvents. The more pronounced decrease of the forward intensity and the sig-

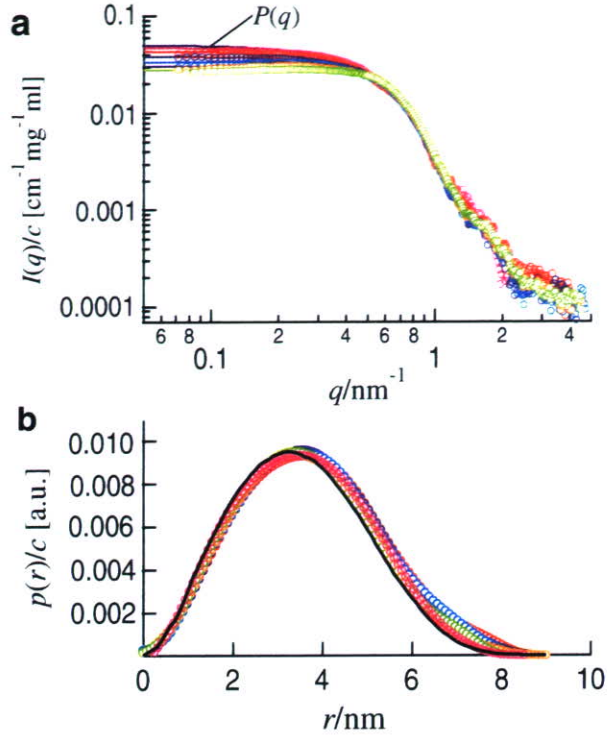

FIG. 1 (color online). (a) The normalized x-ray scattered intensities, $I(q)/c$, and (b) the pair-distance distribution functions, $p(r)$, of rHSA in 0.15M PBS solutions in $3.0 \leq c/\mathrm{mg\,ml^{-1}} \leq 50$. The black solid curve shown in (b) represents $p(r)$ calculated from the crystallography data on HSA [3].

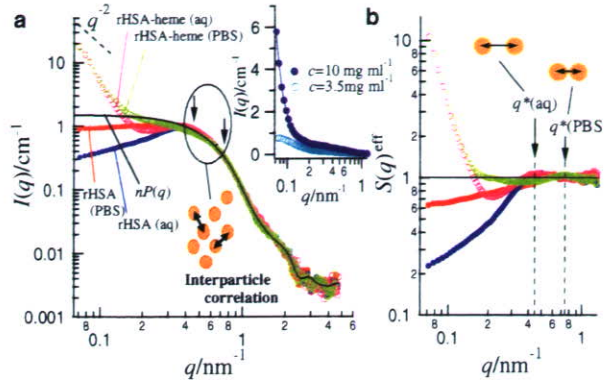

FIG. 2 (color online). (a) Variation of $I(q)$ and (b) the effective structure factors $S^{\mathrm{eff}}(q)$ for rHSA and rHSA-heme in aqueous and 0.15M PBS solutions of a fixed concentration $c = 30\ \mathrm{mg\,ml^{-1}}$. In the inset, the low-$q$ intensities for $c = 3.5\ \mathrm{mg\,ml^{-1}}$ and $c = 10\ \mathrm{mg\,ml^{-1}}$ are compared. Arrows on $S^{\mathrm{eff}}(q)$ highlight the monomer-monomer correlation peak positions q^*.

nificant low-q shift of the monomer-monomer correlation peak position for aqueous rHSA reflect the only weakly screened, thus stronger electrostatic repulsions between the rHSA molecules. Importantly, we observed that heme-incorporated samples exhibit an enhanced forward intensity, which indicates that heme incorporation significantly enhances particle density fluctuations on a large length scale.

Further insights into the spatial correlations between the proteins are gained from the effective structure factors $S^{\mathrm{eff}}(q)$ [11] [Fig. 2(b)]. We extracted $S^{\mathrm{eff}}(q)$ by dividing $I(q)/c$ by $P(q)$ obtained from a dilute rHSA PBS solution. We confirmed that for rHSA-heme, lowering c from 10 to 3.5 $\mathrm{mg\,ml^{-1}}$, leads to a significantly weaker relative low-q intensity, $I(q)/c$, as shown in Fig. 2. In terms of $S^{\mathrm{eff}}(q)$, rHSA under physiological condition still preserves the nature of a repulsively interacting charged colloid but behaves nearly as a hard sphere. If we apply a Yukawa potential model to $S^{\mathrm{eff}}(q)$ with *a priori* input of the solvent ionic strength, the effective protein charge of 18 ± 2 is obtained, being consistent with Ref. [1]. Solutions of rHSA-heme exhibit a similar low-q upturn in $S^{\mathrm{eff}}(q)$, independent of ionic strength. The observation suggests the emergence of a long-range attractive interaction [12,13] between the heme-incorporated rHSA molecules. However, this assignment is only valid when the monodispersity assumption of the protein is fulfilled. In the following, we carefully verify this interpretation, providing convincing evidence for monodispersity of rHSA-heme.

The peak in $S^{\mathrm{eff}}(q)$ arises from protein-protein positional correlations [Fig. 2(b)]. The mean nearest-neighbor distance d^* among the proteins is approximated as $\sim 2\pi/q^*$, where q^* is the scattering vector corresponding to the peak position of $S^{\mathrm{eff}}(q)$. Importantly, q^* is essentially independent before and after heme binding, but it simply depends on the solvent ionic strength related to the screening of the long-range electrostatic repulsion. In Fig. 3, we display a concentration series of $S^{\mathrm{eff}}(q)$ for rHSA and rHSA-heme solutions at different ionic strength. For aqueous rHSA and rHSA-heme, increasing c shifts q^* to higher values, holding a relation $q^* \propto n^{1/3}$ [Fig. 3(e)], where n is the particle number density. The finding clearly shows that both aqueous rHSA and rHSA-heme exhibit a typical feature of charged colloids at low ionic strength, maximizing d^*.

The identical COP (18 mmHg at $c = 50\ \mathrm{mg\,ml^{-1}}$) between the solutions of rHSA-heme and rHSA despite a half value for covalently dimerized rHSA at the same volume fraction [6] also rules out irreversible aggregate formation in rHSA-heme solutions. A simple model calculation demonstrates that a compact aggregate having several tens of aggregation number can never explain the observed low-q feature. No further enhancement of the low-q rise upon screening of the electrostatic repulsion excludes a strong short-range attraction as its origin.

Figure 4 presents complex dielectric spectra of rHSA and rHSA-heme solutions at various c. The relaxation time $\tau_{\mathrm{water}} \sim 8.3$ ps for the high-frequency process common for all solutions reflects the time scale of cooperative rearrangement of the hydrogen-bond network of bulk water [16,18,19]. Besides, the low-frequency relaxation, as-

signed to the rotational diffusion of the proteins [19,20], gives an excellent measure of dimer or higher aggregate formation. The identical relaxation times before and after heme binding, $\tau_{rHSA} \sim 52$–58 ns, provides identical effective molar volume for rHSA and rHSA-heme, $V^{eff} = 4.7 \times 10^4$ cm^3 mol^{-1} ($c \to 0$), according to the Stokes-Einstein-Debye equation, which is very close to the anticipated value of 4.9×10^4 cm^3 mol^{-1} from the molecular mass and specific volume of HSA. This reveals that the freedom of the rotational diffusive motion of the protein is not significantly affected by the heme incorporation.

We point out that in contrast to HSA, well-investigated aqueous lysozyme solutions [11–14,21,22] are already in aggregation regime; even at very low ionic strength, most of lysozyme molecules stick together due to its highly adhesive nature, which is demonstrated by the appearance of the low-q subpeak in $S^{eff}(q)$ and d^* coinciding with the diameter of the protein molecule. Although there arose a controversy as to whether the low-q rise for lysozyme solutions is due to a long-range attraction (LRA) [13,21] or large aggregate formation [22], as for rHSA-heme, the simultaneous observations of the low-q rise in $S^{eff}(q)$ with a host of evidence for monodispersity of the protein, such as d^* far exceeding the contact distance, no additional frictional force on the rotational diffusive motions, identical molecular volume with rHSA, and unbiased COP, provide a plausible argument for the emergence of a LRA. Note that any kind of protein aggregation requires the direct contact between the monomers. Generally, when the repulsion is so strong as to make the particles apart, the low-q rise can be explained only by a LRA [12].

The theoretical $S(q)$ analysis based on a two Yukawa potential model [13] has shown that the relatively longer attraction range than the repulsion one is necessary to produce the so-called zero-q peak in $S(q)$. The more pronounced low-q decrease in $S^{eff}(q)$ for aqueous rHSA is clearly taken over by the deeper dip in $S^{eff}(q)$ for aqueous rHSA-heme, which indicates that the electrostatic repulsion is still active in rHSA-heme solutions and the attraction range is greater than the range of the weakly screened electrostatic repulsion.

For further quantitative description, we tested a two Yukawa model [12,13] for $S^{eff}(q)$ of rHSA-heme. When the attraction range is very long, the model produces a downward convex low-q rise and a huge zero-q intensity reaching more than $\sim$1000 even at small c. However, $S(q)$ starts to rise at $q \leq 0.1$ nm^{-1}, whereas we observed the onset around $q = 0.2$ nm^{-1}. The real expression for a LRA and its potential shape are still not very clear, but the formalism of the potential should significantly affect the low-q shape of $S(q)$. If the system exhibits more slowly decaying attractive potential than the Yukawa decay at small-r, the onset of the low-q rise is expected to shift to higher-q values than that predicted by the Yukawa LRA model.

It is important to recognize that isotropic interaction is not self-evident for any kind of protein system because proteins have irregular shape and inhomogeneously distributed patches by nature. However, until now, almost all experimental and theoretical works on the interactions proteins have been performed based on mean spherical approximation (MSA) and an isotropic interaction assumption [10–15,23]. The recent theoretical work of Bianchi *et al.* [24] revealed that particles interacting with an anisotropic attractive potential can enhance anomalous density fluctuations or gel-network formation even at very low volume fractions. This also implies that anisotropic potentials caused by a site-specific interaction or inhomogeneous distributions of charge or hydrophobic patches may generate unexpectedly drastic effects on the spatial correlations of proteins, where the inherent limitation of small-angle scattering technique lies in the fact that such anisotropic interactions are reduced into one-dimensional $S(q)$. Nevertheless, carefully confirmed monodispersity of rHSA-heme leads us to conclude that our present interpretation based on a LRA is still broadly correct, even if the actual situation is much more complicated, where anisotropic interactions may affect the spatial correlation of the proteins.

Compared to the well-developed short-range attraction and long-range electrostatic repulsion [11,13,23], the general understanding of a LRA of proteins in solution

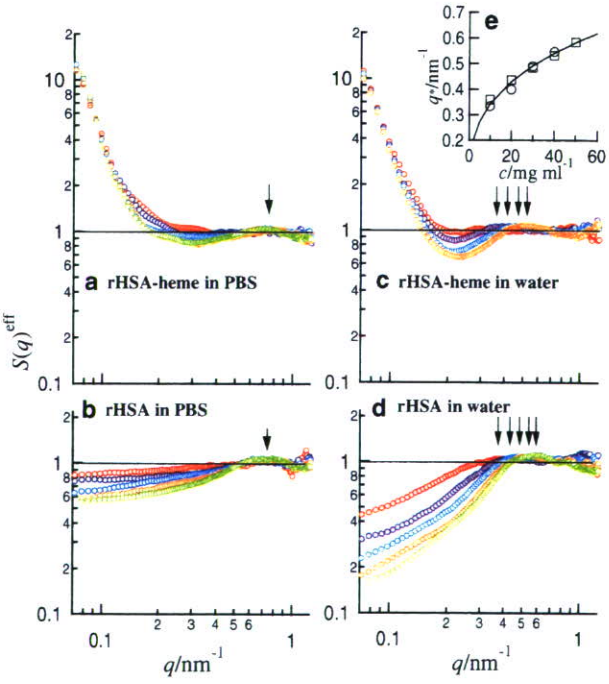

FIG. 3 (color online). Effects of concentration, ionic strength, and heme binding on $S^{eff}(q)$. (a) rHSA-heme and (b) rHSA in 0.15M PBS solutions and (c) rHSA-heme and (d) rHSA in aqueous solutions in $10 \leq c/\text{mg ml}^{-1} \leq 50$ (an increment of 10 mg ml^{-1}). (e) The protein-protein correlation peak position q^* in $S^{eff}(q)$ for aqueous rHSA (□) and rHSA-heme (○) as a function of c.

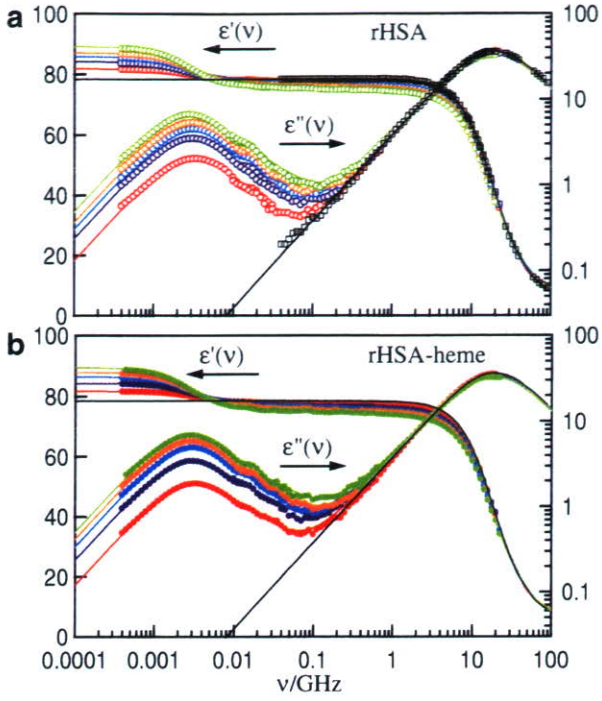

FIG. 4 (color online). Complex dielectric spectra of aqueous solutions of (a) rHSA and (b) rHSA-heme in $10 \leq c/\mathrm{mg\,ml^{-1}} \leq 50$ (an increment of 10 mg ml^{-1} from the bottom) at 25 °C.

[12,13,15] is at an incipient stage. Judging from unbiased $pI(= 4.9)$ and polarization fluctuation amplitudes for rHSA-heme, net charges and their distributions are unlikely to be modified by heme binding, whereas how the occupation of the ligand-binding site allosterically affects the electrostatic interaction of the protein is unclear. The physical origin of a LRA might be entoropic driven, possibly due to modulated hydrophobic patches and their inhomogeneous distributions.

HSA binds heme; the rHSA-heme hybrid takes advantage of this naturally occurring process. In the human body, heme released from methemoglobin is immediately captured by hemopexin or HSA acting as scavengers, and it is efficiently transported to the liver for methabolism [25,26]. Since the emergence of the collective nature of HSAs while preserving the monodispersity could be an efficient way to give the ligand-filled HSA molecules a sort of marker, our data suggest that the heme-bound or -unbound HSAs may be recognized in the bloodstream in terms of the presence and absence of the LRA. Therefore, the optimization of the interparticle potential will be a key to the control of distribution, circulation persistence, and metabolism of functional ligands for medical applications.

This work was partly supported by MEXT, the Grant in Aid for Young Scientists (B) (No. 18740264), and by JSPS, the Grant in Aid for Scientific Research (B) (No. 16350093). T. S. acknowledges the 21st century COE program at Waseda University funded by MEXT. The authors appreciate the strong support of the late Professor Hironobu Kunieda for SAXS measurements and thank Professor Sow-Hsin Chen and Dr. Yun Liu for providing the MATLAB code for two Yukawa model [13].

*Email address: takaaki.sato@waseda.jp
†Email address: eishun@waseda.jp

[1] T. Peters, *All About Albumin: Biochemistry, Genetics, and Medical Applications* (Academic, New York, 1996).
[2] P. A. Zunszain *et al.*, BMC Struct. Biol. **3**, 6 (2003).
[3] X. M. He and D. C. Carter, Nature (London) **358**, 209 (1992).
[4] S. Curry *et al.*, Nat. Struct. Biol. **5**, 827 (1998).
[5] J. Ghuman *et al.*, J. Mol. Biol. **353**, 38 (2005).
[6] T. Komatsu *et al.*, Macromolecules **32**, 8388 (1999).
[7] T. Komatsu, Y. Matsukawa, and E. Tsuchida, Bioconjugate Chemistry **13**, 397 (2002).
[8] T. Komatsu *et al.*, J. Biomed. Mater. Res. **71A**, 644 (2004).
[9] T. Komatsu *et al.*, J. Am. Chem. Soc. **127**, 15 933 (2005).
[10] A. Tardieu *et al.*, J. Cryst. Growth **196**, 193 (1999).
[11] A. Stradner *et al.*, Nature (London) **432**, 492 (2004).
[12] Y. Liu *et al.*, Phys. Rev. Lett. **95**, 118102 (2005).
[13] Y. Liu, W. R. Chen, and S. H. Chen, J. Chem. Phys. **122**, 044507 (2005).
[14] M. Malfois, F. Bonnete, L. Belloni, and A. Tardieu, J. Chem. Phys. **105**, 3290 (1996).
[15] M. G. Noro, N. Kern, and D. Frenkel, Europhys. Lett. **48**, 332 (1999).
[16] T. Sato and R. Buchner, J. Phys. Chem. A **108**, 5007 (2004).
[17] G. Fritz, A. Bergmann, and O. Glatter, J. Chem. Phys. **113**, 9733 (2000).
[18] T. Fukasawa *et al.*, Phys. Rev. Lett. **95**, 197802 (2005).
[19] N. Nandi, K. Bhattacharyya, and B. Bagchi, Chem. Rev. **100**, 2013 (2000).
[20] Y. Hayashi *et al.*, Biophys. J. **79**, 1023 (2000).
[21] Y. Liu *et al.*, Phys. Rev. Lett. **96**, 219802 (2006).
[22] A. Stradner, F. Cardinaux, and P. Schurtenberger, Phys. Rev. Lett. **96**, 219801 (2006).
[23] F. Sciortino *et al.*, Phys. Rev. Lett. **93**, 055701 (2004).
[24] E. Bianchi *et al.*, Phys. Rev. Lett. **97**, 168301 (2006).
[25] V. Jeney, J. W. Eaton, and G. Balla *et al.*, Blood **100**, 879 (2002).
[26] E. Tolosano and F. Altruda, DNA and Cell Biology **21**, 297 (2002).

O_2-Binding Albumin Thin Films: Solid Membranes of Poly(ethylene glycol)-Conjugated Human Serum Albumin Incorporating Iron Porphyrin

Akito Nakagawa,[†] Teruyuki Komatsu,[†,‡,*] Yubin Huang,[†] Gang Lu,[†] and Eishun Tsuchida[†,*]

Research Institute for Science and Engineering, Waseda University, 3-4-1 Okubo, Shinjuku-ku, Tokyo 169-8555 Japan, and PRESTO, Japan Science and Technology Agency (JST), 4-1-8 Honcho, Kawaguchi-shi, Saitama 332-0012, Japan.
Received March 14, 2007; Revised Manuscript Received July 7, 2007

Poly(ethylene glycol) (PEG)-conjugated human serum albumin (HSA) incorporating the tetrakis(α,α,α,α-*o*-amidophenyl)porphinatoiron(II) derivative (FeP) [PEG(HSA−FeP)] is a unique plasma protein-based O_2 carrier as a red blood cell substitute. The aqueous solution of PEG(HSA−FeP) [mw of PEG: 2-kDa (PEG_2) or 5-kDa (PEG_5)] was evaporated on a glass surface to produce a red-colored solid membrane. Scanning electron microscopy observations revealed that the PEG_2(HSA−FeP) membrane consisted of two parts: (i) a surface layer made of a fibrous component (10 μm thickness), and (ii) a bottom layer of an amorphous phase (5 μm thickness). The condensed solution provided a thick membrane (70 μm), which also has the amorphous bottom layer. On the other hand, the PEG_5(HSA−FeP) produced homogeneous membrane made of the fibrous component. The FeP active sites in the solid membrane formed very stable O_2-adduct complexes at 37 °C with a half-lifetime of 40 h. The O_2-binding affinity of the PEG_2(HSA−FeP) membrane ($P_{1/2}$ = 40 Torr, 25 °C) was 4-fold lower than that in aqueous solution, which is kinetically due to the low association rate constant. The membrane was soluble again in water and organic solvents (ethanol and chloroform) without deformation of the secondary structure of the protein. The addition of hyaluronic acid gave a free-standing flexible thin film, and it can also bind and release O_2 as well. These O_2-carrying albumin membranes with a micrometer-thickness would be of significant medical importance for a variety of clinical treatments.

INTRODUCTION

Covalently surface-modified proteins with poly(ethylene glycol) (PEG) show a number of unique properties that make them of interest in a range of practical applications (*1*−*6*). The most beneficial effect of the PEG conjugation from a biological aspect is to confer a nonimmunogenicity to the proteins, rendering them invisible in the body (*7*−*10*). Several classes of protein drugs, such as enzymes and cytokines, have already been approved by the FDA (*4*, *5*), and one of the expected compounds is a PEG-conjugated hemoglobin (PEG-Hb) for use as artificial blood (*11*, *12*). The optimized product has completed a phase I trial and is currently undergoing a phase II safety study (*13*). Second, the PEG modification allows the proteins to be soluble in nonaqueous solvents (benzene, ethanol, and chloroform, etc.) (*14*−*16*). In organic solutions, the proteins exhibited new characteristics, for example, a high thermal stability and a different substrate selectivity. Third, the aqueous PEGylated proteins can be dried on a flat surface to produce solid membranes without any loss of their original activities. However, only limited characterization has been performed on the PEG-conjugated proteins in the solid state.

Recombinant human serum albumin (HSA) incorporating the tetrakis{α,α,α,α-*o*-(1-methylcyclohexanamido)phenyl}-porphinatoiron(II) derivative (FeP, Figure 1) (HSA−FeP) is a unique plasma protein-based O_2 carrier (*17*, *18*). This entirely synthetic hemoprotein can reversibly bind and release O_2 under physiological conditions (pH 7.4, 37 °C) in a fashion similar to Hb. It has also been demonstrated that the surface decoration of HSA−FeP by PEG improved its circulation persistence in the bloodstream (*19*). The PEG(HSA−FeP) is now the most promising material for an entirely synthetic red blood cell substitute.

We have recently found that the aqueous PEG(HSA−FeP) solution cast on the glass surface produces a very smooth solid membrane. The spectroscopic measurements revealed that a reversible O_2 binding to FeP took place in the red-colored membrane. We now report our new findings on the layered film structures of the PEG-conjugated artificial hemoprotein and their O_2-binding behavior.

EXPERIMENTAL PROCEDURES

Materials and Apparatus. All reagents were purchased from commercial sources as special grades and used without further purification. 2-{8-(2-Methylimidazolyl-1-yl)octanoyloxymethyl}-5,10,15,20-tetrakis{α,α,α,α-o-(1-methylcyclohexanamido)-phenyl}porphinatoiron(II) (FeP) was synthesized according to our previously reported procedures (*17*, *20*). Recombinant HSA was provided by the NIPRO Corp. (Osaka, Japan). 2-Iminothiolane hydrochloride (IMT) was purchased from Wako Pure Chemical Industries, Ltd. (Osaka, Japan). α-[3-(3-Maleimido-1-oxopropyl)amino]propyl-ω-methoxy PEG [averaged mw: 2333, Sunbright ME-020MA, PEG_2, and averaged mw: 5207, Sunbright MEMAL-50H, PEG_5) was purchased from the NOF Corp. (Tokyo, Japan). Hyaluronic acid sodium salt (HA, mw: 1.9−2.7 × 10^3 kDa) was a gift from Shiseido Co., Ltd. (Tokyo, Japan). The water was deionized using Millipore Elix and Simpli Lab-UV. The UV−vis absorption spectra were recorded using an Agilent 8453 UV−visible spectrophotometer fitted with an Agilent 89090A temperature control unit. The circular dichroism (CD) spectra were obtained using a JASCO J-820 spectropolarimeter over the range of 200−250 nm.

* Corresponding author. (E.T.) Tel: +81-3-5286-3120, fax: +81-3-3205-4740, e-mail: eishun@waseda.jp. (T.K.) E-mail: teruyuki@waseda.jp.
† Waseda University.
‡ Japan Science and Technology Agency.

10.1021/bc070086m CCC: $37.00
Published on Web 08/16/2007

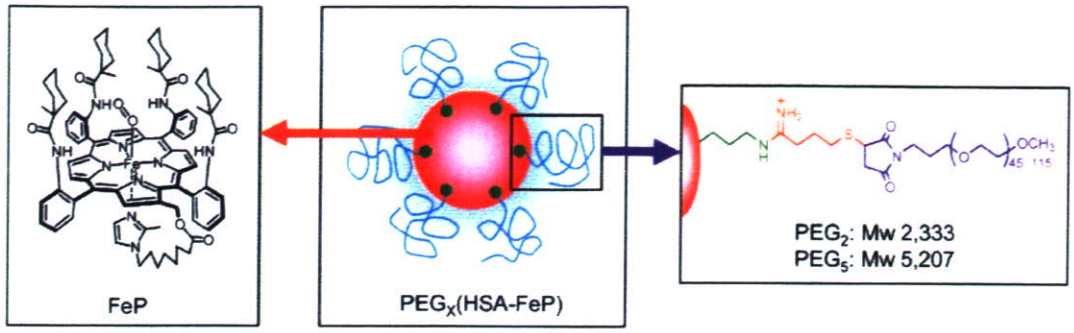

Figure 1. Structure of the PEG$_X$(HSA−FeP) molecule.

Preparation of PEG$_X$(HSA−FeP) Solid Membranes. The phosphate-buffered saline (PBS) solutions of PEG$_X$(HSA−FeP) (X = 2 or 5) were prepared with IMT and PEG$_X$ (pH 7.4, [HSA] = 5 wt %, FeP/HSA = 4/1 (mol/mol)) according to our previously reported methods (*19*). The binding number of the PEG$_X$ chain on the HSA−FeP surface was determined by the MALDI-TOF MS spectra (*19*). The PBS solution was dialyzed using a Spectra/Por 1 regenerated cellulose dialysis membrane (MWCO: 6−8 kDa, Spectrum Labratories, Inc.) against the pure water to remove any included electrolytes. The obtained aqueous solution of PEG$_X$(HSA−FeP) (CO adduct complex, 0.5 mL) was spread on a glass plate [30 × 40 mm, thickness: 0.12−0.17 mm, Matsunami Glass Ind., Ltd. (Osaka, Japan)] and evaporated at an ambient temperature in the dark for 12 h, which produced a red-colored transparent solid membrane.

For the scanning electron microscopy measurements, the samples on the glass plate were sputtered with Pd−Pt using a Hitachi E-1030 ion sputter. The SEM observations were performed using a Hitachi S-4500S field emitted scanning electron microscope.

Furthermore, 0.5 mL of an aqueous solution of hyaluronic acid (HA, 0.2, 0.4, 0.6, 0.8, 1.0 wt %) was added to the PEG$_2$-(HSA−FeP) solution (CO adduct complex, 0.5 mL, [HSA] = 5 wt %). The mixture was poured into a poly(styrene) balance dish (44 × 44 × 15 mm) and dried at room temperature in the dark. After 12 h, the formed membrane was gently peeled off and characterized.

The water content of the solid membrane was measured by thermogravimetric-differential thermal analysis using a Rigaku TG8120 instrument at a hearing rate of 10 °C/min.

O_2-Binding Parameters. The O_2 binding to PEG$_X$(HSA−FeP) is expressed by eq 1,

$$\text{PEG}_X(\text{HSA}-\text{FeP}) + \text{O}_2 \underset{k_{off}}{\overset{k_{on}}{\rightleftharpoons}} \text{PEG}_X(\text{HSA}-\text{FeP}(\text{O}_2)) \quad (1)$$

where the O_2 binding equilibrium constant $K = k_{on}/k_{off}$.

The PEG$_X$(HSA−FeP) membrane or PEG$_2$(HSA−FeP)/HA hybrid membrane on the glass plate was placed in a 1-cm quartz cuvette for the spectral measurements, which was sealed tightly with a rubber septa. The O_2-binding affinity (gaseous partial pressure at which 50% of FeP was dioxygenated, $P_{1/2} = 1/K$) was determined by the spectral changes at various O_2/N_2 pressures (*17*, *19*, *20*). The UV−vis absorption spectra were recorded within the range of 350−700 nm. The half-lifetime of the autoooxidation of the FeP(O_2) complex was determined by the time-course of the absorption change at 426 nm. The association and dissociation rate constants for O_2 (k_{on}, k_{off}) to the PEG$_X$(HSA−FeP) membrane or PEG$_2$(HSA−FeP)/HA hybrid membrane were measured by a competitive rebinding technique using a Unisoku TSP-1000WK laser flash photolysis instrument (*17*, *19*, *20*).

Figure 2. Photograph of the PEG$_2$(HSA−FeP) solid membrane on the glass plate.

RESULTS AND DISCUSSION

Structure of PEG$_X$(HSA−FeP) Membrane. The PEGylation of HSA−FeP (FeP/HSA = 4/1 (mol/mol)) was readily accomplished under mild conditions using the commercially available IMT and maleimide-terminated PEG (*19*). The average number of the PEG chain on the HSA−FeP surface was modulated to 6.0; the viscosity and colloid osmotic pressure of the PBS solution of this molecule ([HSA] = 5 wt %) satisfied the clinical requirements of a red blood cell substitute (*19*). The solution was subsequently desalted by dialysis against pure water and spread on the glass plate. After drying overnight at room temperature, a red-colored transparent solid membrane was formed (Figure 2). The HSA−FeP without the PEG modification did not produce such a homogeneous thin film, only affording a brittle membrane with many cracks.

Scanning electron microscopy observations of the PEG$_2$-(HSA−FeP) membrane showed a uniform thickness of 15 μm and a very smooth surface [Figure 3a,b)]. From a careful inspection of the side-view, we found that the membrane consists of two parts: (i) the surface layer with a thickness of 10 μm made of a highly oriented fibrous component, and (ii) the bottom layer with a thickness of 5 μm made of an amorphous phase (Figure 3b). Cutting the glass plate with a lateral force, the PEG$_2$-(HSA−FeP) membrane was extended and produced long fibers with a width of 350 nm (Figure 3c). The condensed solution ([HSA] = 15 wt %) provided a thick membrane with a thickness of 70 μm, which also has the amorphous bottom layer of 5 μm (Figure 3d). Interestingly, the membrane prepared on the poly-(styrene) dish was mainly composed of the amorphous layer; the surface fibrous phase was less than 20% (Figure 3e). On the other hand, water evaporation of the PEG$_5$(HSA−FeP) solution ([HSA] = 5 wt %) on the glass surface provided a homogeneous membrane, which is made of the fibrous component. The precise mechanism of the fiber formation during the water evaporation process is still not clear, but our results show that the structure of the PEG$_X$(HSA−FeP) membrane is very dependent on the surface feature of the substrate and the chain length of the PEG.

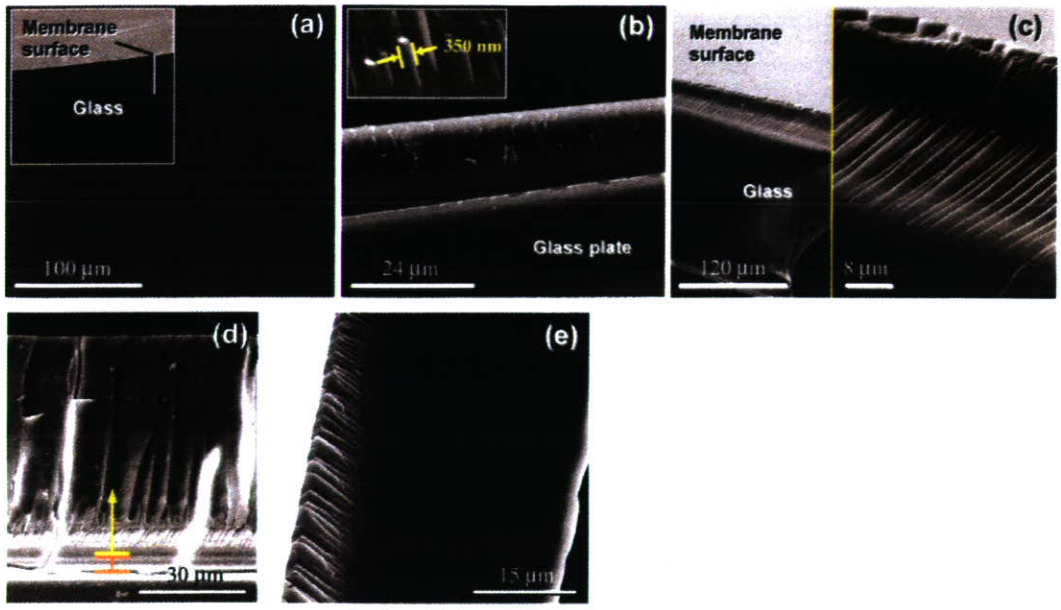

Figure 3. SEM images of the PEG_2(HSA−FeP) membrane on the glass plate. (a) Top-view of the very smooth surface without any crack. (b) Side-view of the membrane section, showing a surface layer made of fibrous component and a bottom layer made of an amorphous phase. (c) Extended nanofiber structure of the surface layer. (d) Thick membrane with a 5 μm amorphous bottom layer (indicated by orange bars) on the glass surface. (e) Membrane prepared on the poly(styrene) surface.

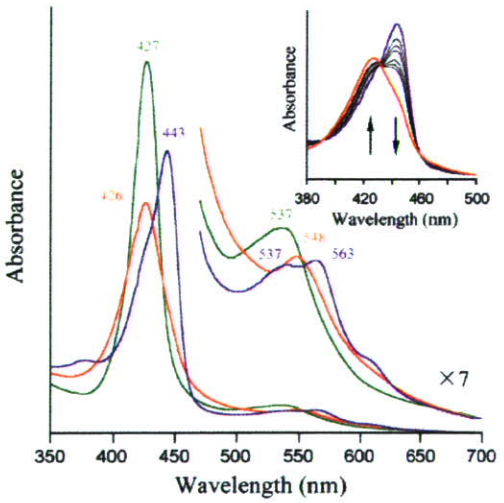

Figure 4. UV−vis absorption spectral changes of the PEG_2(HSA−FeP) membrane on the glass plate at 25 °C (blue line: under N_2, red line: under O_2, green line: under CO). The inset shows the spectral changes at various O_2-partial pressures (P_{O_2}: 0, 10, 19, 30, 76, 114, 152, 760 Torr from blue to red line).

O_2-Binding Properties. The UV−vis absorption spectrum of the PEG_X(HSA−FeP) membrane showed an absorption maxima (λ_{max}) at 427 and 537 nm, indicating the formation of the CO-coordinate low-spin state of FeP (Figure 4) (*17, 19*−*21*). This suggested that the ferrous carbonyl complex was retained during the water evaporation for 12 h at an ambient temperature. Light irradiation to the membrane using a 500-W halogen lamp under a 100% O_2 for 20 min led to the CO dissociation and O_2-adduct complex formation of FeP (λ_{max}: 426, 548 nm). By flowing N_2 to the membrane in the quartz cuvette, the UV−vis absorption spectrum shifted to that of a high-spin ferrous complex with an intramolecularly coordinated 2-methylimidazolyl group (λ_{max}: 443, 537, 563 nm). These spectral changes were repeatedly observed and found dependent on the O_2-partial pressure (0 Torr ↔ 760 Torr), which demonstrated that the reversible dioxygenation of FeP took place in the membrane. The half-lifetime of the autoxidation ($\tau_{1/2}$) of the FeP(O_2) to Fe^{3+}P was 40 h at 37 °C, which is 3-fold longer than the value in the PBS solution.

The O_2-binding affinity of the PEG_2(HSA−FeP) membrane ($P_{1/2}$ = 40 Torr, 25 °C) determined from the UV−vis absorption spectral changes at various O_2/N_2 pressures (Figure 4 inset) was 4-fold lower (high $P_{1/2}$) than that of the monomeric PEG_2(HSA−FeP) in water (Table 1). Since the O_2 coordination to the Fe porphyrin is an exothermic reaction, the O_2-binding affinity of the membrane decreased at 37 °C ($P_{1/2}$ = 61 Torr). In contrast, PEG_5(HSA−FeP) membrane showed the identical O_2-bidnig affinity to that in aqueous PBS solution ($P_{1/2}$ = 11 Torr, 25 °C).

In order to elucidate the O_2-binding kinetics of the PEG_X-(HSA−FeP) membrane, flash photolysis experiments were carried out. The time course of the absorption change after the laser pulse irradiation to the PEG_2(HSA−FeP) membrane in the quartz cuvette exhibited two first-order kinetics. We previously reported that the binding processes of O_2 to HSA−FeP and PEG_X(HSA−FeP) in aqueous media were fitted to a double-exponential expression, giving two different association rate constants for the fast and slow reactions (k_{on} and k'_{on}) (*19, 22*). It has been interpreted that the O_2 recombination to FeP in the protein could be affected by the each nanoscopic environment around the accommodation site, for example, a steric hindrance of the amino acid residue and difference in polarity. The k'_{on} was used to be approximately one-third of the k_{on} (*17, 19, 22*). Nevertheless, the ratio of k'_{on}/k_{on} observed in the PEG_2-(HSA−FeP) membrane was less than one-tenth (Table 1). We then theorized that this can be attributed to the O_2 diffusion in the two parts of the membrane. In the major surface layer of the fibrous component, the diffusion of the O_2 could be slower than in water, and it could be much slower in the amorphous bottom phase. The following results support our assumption. (i) The thickness ratio of the two layers (10 μm/5 μm = 2.0) corresponds well to the molar ratio of the k_{on} and k'_{on} (= 2.1). (ii) The absorption decay accompanied with the O_2 rebinding

Table 1. O_2-Binding Parameters of Solid Membranes of PEG_X(HSA−FeP) at 25 °C

system	k_{on} ($Torr^{-1}\,s^{-1}$)	k'_{on} ($Torr^{-1}\,s^{-1}$)	k_{off} (s^{-1})	k'_{off} (s^{-1})	$P_{1/2}$ (Torr)[a]
PEG_2(HSA−FeP) solution[b]	20	7.5	1.7×10^2	70	11 [32]
PEG_5(HSA−FeP) solution[b]	20	10	1.7×10^2	90	11 [31]
PEG_2(HSA−FeP) membrane	5.7	0.54	2.3×10^2	22	40 [61]
PEG_5(HSA−FeP) membrane	3.1		34		11 [33]
PEG_2(HSA−FeP)/HA membrane	4.3	0.22	1.4×10^2	7	32 [60]
Hb solution (T-state)[c]	4.8		1.8×10^2		40
Hb/maltose membrane[d]	1.2×10^{-13}		8.3×10^{-11}		760

[a] At 37 °C in brackets [ ]. [b] In PBS solution (pH 7.4), ref 19. [c] In 50 mM potassium phosphate buffer (pH 7.0) at 20 °C, ref 24. [d] Reference 23.

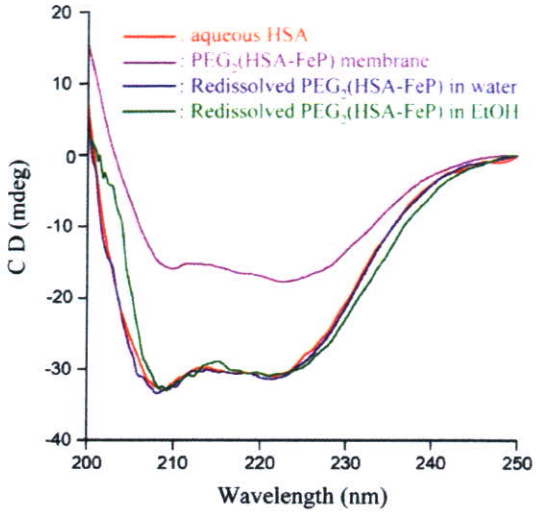

Figure 5. CD spectra of PEG_2(HSA−FeP) at various conditions at 25 °C.

to the PEG_5(HSA−FeP) membrane, which consists of the homogeneous fibrous layer, was fitted by single exponential, giving only one association rate constant k_{on}.

The low O_2-binding affinity of the solid membrane of PEG_2-(HSA−FeP) compared to that in the PBS solution is kinetically due to the low association rate constants (Table 1). Even though this result was in significant contrast to the fact that the similar solid membrane of human Hb with maltose (Hb/maltose = 6/4, wt/wt) could not bind O_2 under the same conditions, its O_2-binding affinity was extremely low ($P_{1/2}$ = 760 Torr) (*23*). Since the quaternary structure of Hb was restrained in the solid form, its tense-state conformation cannot change to a relaxed-state with a high O_2-binidng affinity (*24*). In the PEG_X(HSA−FeP) membrane, the protein scaffold was solidified by a bulk water evaporation; however, it would not dramatically influence the dioxygenation of FeP, because the O_2-binding equilibrium is not synchronized with the quaternary structure of the HSA matrix.

PEG_X(HSA−FeP) in Organic Solutions. We have found that the PEG modification enables HSA−FeP to dissolve in organic solvents. The red-colored PEG_X(HSA−FeP) membrane was homogeneously soluble not only in water but also in ethanol and chloroform. The CD spectrum of the membrane showed a different pattern compared to that in aqueous media (Figure 5). The intensity ratio of the double minimum peaks at 208 and 222 nm (I_{208}/I_{222}) of rHSA or PEG_X(HSA−FeP) is normally 1.1 (*25*, *26*), while the membrane showed 0.9. Interestingly, the redissolved aqueous and ethanol solutions both showed the same spectra as the original aqueous HSA. This result implies that the change of the secondary structure in the protein in the solid and liquid states is reversible. The ethanolic PEG_X(HSA−FeP) also exhibited the same absorption changes upon exposure to O_2 and N_2. These organic solutions can also be cast on a glass surface to form identical PEG_X(HSA−FeP) membranes.

PEG_2(HSA−FeP) Membrane with Hyaluronic Acid. An attempt to isolate the PEG_X(HSA−FeP) membrane from the glass surface unfortunately failed, because it was rather fragile, when peeled off. We then added a supporting polymer to the protein solution and prepared the solid membrane on a glass plate or a poly(styrene) dish. Hyaluronic acid (HA), which is known as a glycosaminoglycan component of connective tissues, hyaline body and extracellular matrix, was selected as the biocompatible polymer support (*27*). We also expected that the high water retention capability of HA may have a positive effect on retarding the proton-driven oxidation of the FeP(O_2) complex. Water evaporation of the PEG_2(HSA−FeP)/HA mixture [0.5 mL/0.5 mL, total [HSA] = 2.5 wt %, total [HA] = 0.2 wt %] on the glass plate or poly(styrene) dish produced the red-colored uniform solid membranes. It could not be isolated from the glass plate but was easily peeled off from the poly(styrene) surface, providing a free-standing thin film of the PEG_2(HSA−FeP)/HA hybrid [Figure 6a]. The formation of the flexible film was quite dependent on the HA content. When the total concentration of HA is 0.2−0.5 wt %, we could readily obtain the membrane from the plastic surface. The SEM observations of the film showed that it was made of a homogeneous layer with a relatively coarse structure (Figure 6b). In contrast, the film cast on the glass plate consists of the two-layered form: a major course phase and bottom dense phase (Figure 6c). This implies

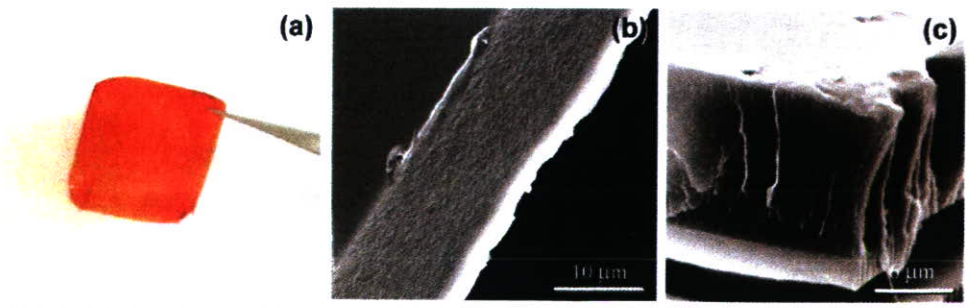

Figure 6. PEG_2(HSA−FeP)/HA membrane. (a) Photograph of the free-standing flexible film, which is prepared on the poly(styrene) surface. (b) SEM of the isolated film. (c) SEM of the membrane prepared on the glass surface.

that the membrane structure of the PEG_2(HSA−FeP)/HA is also influenced by the surface properties of the substrate.

The UV−vis absorption spectral pattern reversibly changed from that of the five-N-coordinate high-spin ferrous complex under an N_2 atmosphere (λ_{max}: 445, 540, 566 nm) to that of the O_2-adduct complex under an O_2 atmosphere (λ_{max}: 426, 545 nm). The O_2-binding parameters of the PEG_2(HSA−FeP)/HA membrane showed a tendency similar to the PEG_2(HSA−FeP) film; the low O_2-binding affinity ($P_{1/2}$ = 32 Torr, 25 °C) is mainly due to the slow association rate constant (Table 1). The half-life of the O_2-adduct complex was 40 h at 37 °C; we could not see any water retention effect of HA that could prolong the stability of FeP(O_2). The water content of the PEG_2(HSA−FeP) membrane and PEG_2(HSA−FeP)/HA membrane were determined by the differential thermal analyses to be 6.5 wt % and 6.6 wt %, respectively.

CONCLUSIONS

The stable solid membranes of a PEGylated artificial hemoprotein have been prepared, and their O_2-binding properties were physicochemically characterized in relation to the layer morphology. The red-colored thin film is soluble again in water and organic solvents (ethanol, chloroform) without any deformation of the secondary structure of the protein. The addition of hyaluronic acid as the polymer support gave the free-standing flexible film. These O_2-binding albumin membranes are a red blood cell substitute with a micrometer-thickness that can be preserved anywhere (e.g., on a shelf and in an ambulance) and reproduced as a saline solution at anytime (e.g., at the scene of a disaster). Furthermore, it would be of great medical importance for a variety of clinical treatments, such as O_2-enriched coating agents for medical devices or artificial organs and an O_2-transporting adhesive plaster for wound healing.

ACKNOWLEDGMENT

This work was partially supported by a Grant-in-Aid for Scientific Research (No. 16350093, No. 18750156) from JSPS, PRESTO, and from JST, and Health Science Research Grants from MHLW, Japan.

LITERATURE CITED

(1) Harris, J. M., Martin, N. E., and Modi, M. (2001) Pegylation—a novel process for modifying pharmacokinetics. *Clin. Pharmacokinet. 40*, 539−551.

(2) Veronese, F. M., and Harris, J. M. (2002) Introduction and overview of peptide and protein PEGylation. *Adv. Drug Delivery Rev. 54*, 453−456.

(3) Roberts, M. J., Bentley, M. D., and Harris, J. M. (2002) Chemistry for peptide and protein PEGylation. *Adv. Drug Delivery Rev. 54*, 459−476.

(4) Veronese, F. M. (2001) Peptide and protein PEGylation: a review of problems and solutions. *Biomaterials 22*, 405−417.

(5) Veronese, F. M., and Pasut, G. (2005) PEGylation, successful approach to drug delivery. *Drug Discovery Today 10*, 1451−1455.

(6) Nucci, M. L., Shorr, R., and Abuchowski, A. (1991) The therapeutic value of poly(ethylene glycol) modified proteins. *Adv. Drug Delivery Rev. 6*, 133−151.

(7) Abuchowski, A., van Es, T., Palzuk, N. C., and Davis, F. F. (1977) Alteration of immunological properties of bovine serum albumin by covalently attachment of polyethylene glycol. *J. Biol. Chem. 252*, 3578−3581.

(8) Abuchowski, A., McCoy, J. R., Palczuk, N. C., van Es, T., and Davis, F. F. (1977) Effect of covalently attachment of polyethylene glycol on immunogenicity and circulating life of bovine liver catalase. *J. Biol. Chem. 252*, 3582−3586.

(9) He, X. H., Shaw, P. C., and Tam, S. C. (1999) Reducing the immunogenicity and improving the in vivo activity of trichosanthin by site-directed PEGylation. *Life Sci. 65*, 355−368.

(10) Hinds, K. D., and Kim, S. W. (2002) Effects of PEG conjugation on insulin properties. *Adv. Drug Delivery Rev. 54*, 505−530.

(11) Vandegriff, K. M., Malavalli, A., Wooldbridge, J., Lohman, J., and Winslow, R. M. (2003) MP4, a new nonvasoactive PEG-Hb conjugate. *Transfusion 43*, 509−516.

(12) Manjula, B. M., Tsai, A., Upadhya, R., Perumalsamy, K., Smith, P. K., Malavalli, A., Vandegriff, K., Winslow, R. M., Intaglietta, M., Prabhakaran, M., Friedman, J. M., and Acharya, A. S. (2003) Site-specific PEGylation of hemoglobin at Cys-93(β): correlation between the colligative properties of the PEGylated protein and the length of the conjugated PEG chain. *Bioconjugate Chem. 14*, 464−472.

(13) Olofsson, C., Ahl, T., Johansson, T., Larsson, S., Nellgard, P., Ponzer, S., Fagrell, B., Przybelski, R., Keipert, P., Winslow, N., and Winslow, R. M. (2006) A multicenter clinical study of the safety and activity of maleimide-polyethylene glycol-modified hemoglobin (hemospan) in patients undergoing major orthopedic surgery. *Anesthesiology 105*, 1153−1163.

(14) Takahashi, K., Ajima, A., Yoshimoto, T., and Inada, Y. (1984) Polyethylene glycol-modified catalase exhibits unexpectedly high activity in benzene. *Biochem. Biophys. Res. Commun. 125*, 761−766.

(15) Kawahara, N. Y., and Ohno, H. (1997) Induced thermostability of poly(ethylene oxide)-modified hemoglobin in glycols. *Bioconjugate Chem. 8*, 643−648.

(16) Wiwatchaiwong, S., Nakamura, N., and Ohno, H. (2006) Spectroscopic characterization and electrochemistry of poly(ethylene oxide)-modified myoglobin in organic solvents. *Biotechnol. Prog. 22*, 1276−1281.

(17) Komatsu, T., Matsukawa, Y., and Tsuchida, E. (2002) Effect of heme structure on O_2-binding properties of human serum albumin−heme hybrids: intramolecular histidine coordination provides a stable O_2-adduct complex. *Bioconjugate Chem. 13*, 397−402.

(18) Komatsu, T., Yamamoto, H., Huang, Y., Horinouchi, H., Kobayashi, K., and Tsuchida, E. (2004) Exchange transfusion with synthetic oxygen-carrying plasma protein "albumin-heme" into an acute anemia rat model after seventy-percent hemodilution. *J. Biomed. Mater. Res. A 71A*, 644−651.

(19) Huang, Y., Komatsu, T., Wang, R.-M., Nakagawa, A., and Tsuchida, E. (2006) Poly(ethylene glycol)-conjugated human serum albumin including iron porphyrins: surface modification improves the O_2-transporting ability. *Bioconjugate Chem. 17*, 393−398.

(20) Tsuchida, E., Komatsu, T., Kumamoto, S., Ando, K., and Nishide, H. (1995) Synthesis and O_2-Binding properties of tetraphenylporphyrinatoiron(II) derivatives bearing a proximal imidazole covalently bound at the β-pyrrolic position. *J. Chem. Soc., Perkin Trans. 2*, 747−753.

(21) Collman, J. P., Brauman, J. I., Iverson, B. L., Sessler, J. L., Morris, R. M., and Gibson, Q. H. (1983) O_2 and CO binding to iron(II) porphyrins: a comparison of the "picket fence" and "pocket" porphyrins. *J. Am. Chem. Soc. 105*, 3052−3064.

(22) Komatsu, T., Matsukawa, Y., and Tsuchida, E. (2000) Kinetics of CO and O_2 binding to human serum albumin−heme hybrid. *Bioconjugate Chem. 11*, 772−776.

(23) Chung, J. E., Sakai, H., Takeoka, S., Nishide, H., and Tsuchida, E. (1995) Coordination behavior of O_2 and CO in a solid film consisting of hemoglobin and maltose. *Bull. Chem. Soc. Jpn. 68*, 1006−1011.

(24) Sawicki, C. A., and Ginson, Q. H. (1977) Properties of the T state of human oxyhemoglobin studied by laser photolysis. *J. Biol. Chem. 252*, 7538−7547.

(25) Nakajou, K., Watanabe, H., Kragh-Hansen, U., Maruyama, T., and Otagiri, M. (2003) The effect of glycation on the surface on the structure, function and biological fate of human serum albumin as revealed by recombinant mutants. *Biochim. Biophys. Acta 1623*, 88−97.

(26) Peters, T. (1996) *All about albumin: biochemistry, genetics and medical applications*; Academic Press, San Diego.

(27) Goa, K. L., and Benfield, P. (1994) Hyaluronic-acid −a review of its pharmacology and use as a surgical and in ophthalmology, and its therapeutic potential in joint disease and wound-healing. *Drugs 47*, 536−566.

BC070086M

J|A|C|S
ARTICLES
Published on Web 08/18/2007

Genetic Engineering of the Heme Pocket in Human Serum Albumin: Modulation of O_2 Binding of Iron Protoporphyrin IX by Variation of Distal Amino Acids

Teruyuki Komatsu,*,†,‡ Akito Nakagawa,† Patricia A. Zunszain,‖ Stephen Curry,‖ and Eishun Tsuchida*,†

Contribution from the Research Institute for Science and Engineering, Waseda University, 3-4-1 Okubo, Shinjuku-ku, Tokyo 169-8555, Japan, PRESTO, Japan Science and Technology Agency, 4-1-8 Honcho, Kawagichi-shi, Saitama 332-0012, Japan, and Division of Cell and Molecular Biology, Faculty of Natural Sciences, Imperial College London, South Kensington Campus, London SW7 2AZ, United Kingdom

Received June 8, 2007; E-mail: teruyuki@waseda.jp; eishun@waseda.jp

Abstract: Complexing an iron protoporphyrin IX into a genetically engineered heme pocket of recombinant human serum albumin (rHSA) generates an artificial hemoprotein, which can bind O_2 in much the same way as hemoglobin (Hb). We previously demonstrated a pair of mutations that are required to enable the prosthetic heme group to bind O_2 reversibly: (i) Ile-142 → His, which is axially coordinated to the central Fe^{2+} ion of the heme, and (ii) Tyr-161 → Phe or Leu, which makes the sixth coordinate position available for ligand interactions [I142H/Y161F (HF) or I142H/Y161L (HL)]. Here we describe additional new mutations designed to manipulate the architecture of the heme pocket in rHSA–heme complexes by specifically altering distal amino acids. We show that introduction of a third mutation on the distal side of the heme (at position Leu-185, Leu-182, or Arg-186) can modulate the O_2 binding equilibrium. The coordination structures and ligand (O_2 and CO) binding properties of nine rHSA(triple mutant)–heme complexes have been physicochemically and kinetically characterized. Several substitutions were severely detrimental to O_2 binding: for example, Gln-185, His-185, and His-182 all generated a weak six-coordinate heme, while the rHSA(HF/R186H)–heme complex possessed a typical bis-histidyl hemochrome that was immediately autoxidized by O_2. In marked contrast, HSA(HL/L185N)–heme showed very high O_2 binding affinity ($P_{1/2}^{O_2}$ 1 Torr, 22 °C), which is 18-fold greater than that of the original double mutant rHSA(HL)–heme and very close to the affinities exhibited by myoglobin and the high-affinity form of Hb. Introduction of Asn at position 185 enhances O_2 binding primarily by reducing the O_2 dissociation rate constant. Replacement of polar Arg-186 with Leu or Phe increased the hydrophobicity of the distal environment, yielded a complex with reduced O_2 binding affinity ($P_{1/2}^{O_2}$ 9–10 Torr, 22 °C), which nevertheless is almost the same as that of human red blood cells and therefore better tuned to a role in O_2 transport.

Introduction

In the human circulatory system, iron(III) protoporphyrin IX (hemin) released from methemoglobin (metHb) is captured by a specific glycoprotein, hemopexin (Hpx, 60 kDa), which binds it with very high affinity ($> 10^{13}$ M^{-1}).[1,2] Nevertheless, due to the extremely low abundance of Hpx in the blood stream (~17 μM), human serum albumin (HSA, 66.5 kDa, 640 μM) acts as a depot of hemin under pathological conditions of trauma and severe hemolysis.[3] HSA is the most prominent plasma protein and has a remarkable ability to bind a broad range of insoluble endogenous and exogenous compounds, such as fatty acids, hemin, bilirubin, bile acids, thyroxine, and a wide variety of drugs.[4,5] This heart-shaped carrier protein is composed of three structurally similar domains (I–III), each of which contains two subdomains (A and B).[6,7] Recent crystallographic studies revealed that the hemin is bound within a narrow D-shaped hydrophobic cavity in subdomain IB (Figure 1a).[8,9] The central iron atom is weakly coordinated by Tyr-161 and the porphyrin propionate side chains interact with a triad of basic amino acid

† Waseda University.
‡ JST.
‖ Imperial College London.

(1) (a) Muller-Eberhard, U; Grizzuti, K. *Biochemistry* **1971**, *10*, 2062–2066. (b) Muller-Eberhard, U.; Morgan, W. T. *Ann. N.Y. Acad. Sci.* **1975**, *244*, 624–650.
(2) Paoli, M.; Anderson, B. F.; Baker, H. M.; Morgan, W. T.; Smith, A.; Baker, E. N. *Nat. Struct. Biol.* **1999**, *6*, 926–931.
(3) Tolosano, E.; Altruda, F. *DNA Cell Biol.* **2002**, *21*, 297–306.
(4) Peters, T. *All about Albumin: Biochemistry, Genetics and Medical Applications*; Academic Press: San Diego, CA, 1996; and references therein.
(5) (a) Kragh-Hansen, U. *Pharmacol. Rev.* **1981**, *33*, 17–53. (b) Kragh-Hansen, U. *Danish Med. Bull.* **1990**, *37*, 57–84.
(6) (a) He, X. M.; Carter, D. C. *Nature* **1992**, *358*, 209–215. (b) Carter, D. C.; Ho, J. X. *Adv. Protein Chem.* **1994**, *45*, 153–203.
(7) (a) Curry, S.; Madelkow, H.; Brick, P.; Franks, N. *Nat. Struct. Biol.* **1998**, *5*, 827–835. (b) Bhattacharya, A. A.; Grune, T.; Curry, S. *J. Mol. Biol.* **2000**, *303*, 721–732.
(8) Wardell, M.; Wang, Z.; Ho, J. X.; Robert, J.; Ruker, F.; Rubel, J.; Carter, D. C. *Biochem. Biophys. Res. Commun.* **2002**, *291*, 813–819.
(9) Zunszain, P. A.; Ghuman, J.; Komatsu, T.; Tsuchida, E.; Curry, S. *BMC Struct. Biol.* **2003**, *3*, 6.

10.1021/ja074179q CCC: $37.00

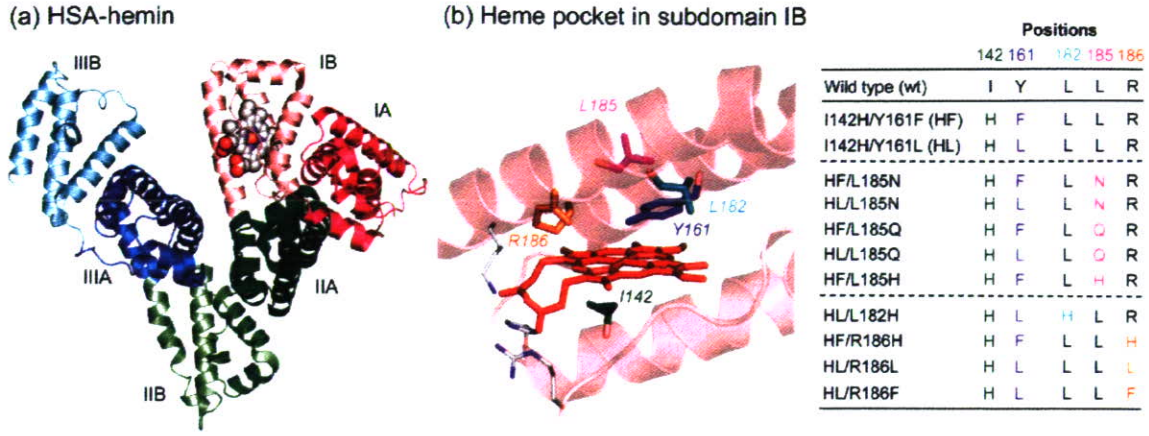

	Positions				
	142	161	182	185	186
Wild type (wt)	I	Y	L	L	R
I142H/Y161F (HF)	H	F	L	L	R
I142H/Y161L (HL)	H	L	L	L	R
HF/L185N	H	F	L	N	R
HL/L185N	H	L	L	N	R
HF/L185Q	H	F	L	Q	R
HL/L185Q	H	L	L	Q	R
HF/L185H	H	F	L	H	R
HL/L182H	H	L	H	L	R
HF/R186H	H	F	L	L	H
HL/R186L	H	L	L	L	L
HL/R186F	H	L	L	L	F

Figure 1. (a) Crystal structure of HSA−hemin complex (1O9X) from ref 9. Hemin is shown in a space-filling representation. (b) Heme pocket structure in subdomain IB and positions of amino acids where site-specific mutations were introduced. The essential double mutations to confer O_2 binding capability to the heme group are I142H and Y161F (or Y161L). Abbreviations of the triple mutants are shown in the table.

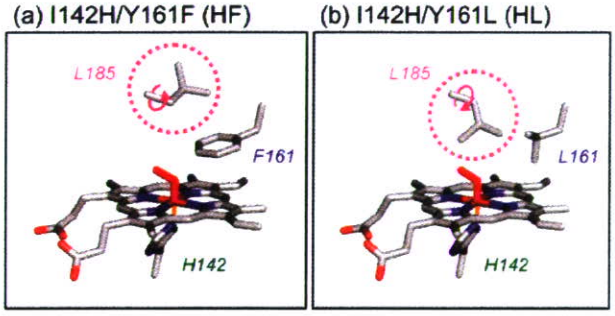

Figure 2. Structural models of the heme pocket in dioxygenated (a) rHSA-(HF)−heme and (b) rHSA(HL)−heme: distal-side steric effect of Leu-185 on O_2 and CO association.[20]

residues at the entrance (Arg-114, His-146, and Lys-190) (Figure 1b). In terms of the general hydrophobicity of the α-helical heme pocket, subdomain IB of HSA has broadly similar features to the globin-wrapping heme in Hb and myoglobin (Mb). If the HSA-based O_2 carrier is realized, it has the potential of acting not only as a red blood cell (RBC) substitute but also as an O_2-providing therapeutic reagent. However, the reduced ferrous HSA−heme would be immediately autoxidized by O_2, because HSA lacks the proximal histidine that in Hb and Mb allows the prosthetic heme group to bind O_2.[10] On the basis of the detailed structure of the heme binding site of HSA, we introduced a His into the Leu-142 position by site-directed mutagenesis that provides axial coordination to the central Fe^{2+} atom of the heme, and we replaced the coordinated Tyr-161 by Phe or Leu, neither of which can interact with the Fe^{2+} ion (Figure 2).[11] This mutagenic approach produced the recombinant HSA(I142H/Y161F)−heme [rHSA(HF)−heme] and HSA(I142H/Y161L)−heme [rHSA(HL)−heme] complexes; these artificial hemoproteins can bind and release O_2 at room temperature, although the O_2 binding affinity of rHSA−heme is at least an order of magnitude lower than that of Hb(α) (R-state).[11] To develop this promising O_2-carrying plasma protein as a blood substitute, further work is required to regulate the O_2 binding affinity suitable for Hb, Mb, and human RBC.

In Hb and Mb, His-64 on the distal side of the heme has been conserved during evolution and plays an important role for tuning their ligand affinities. A neutron diffraction study of MbO_2 clearly showed that the N−H bond of the distal His-64 is restrained from optimal alignment for strong hydrogen bonding with the coordinated O_2.[12] Olson et al.[13a] reported that the substitution of Gly for His-64 in Mb and Hb(α) caused a significant decrease in the O_2 binding affinity due to an ~100-fold increase in the O_2 dissociation rate constant. A number of systematic investigations of site-directed mutants of Hb and Mb have shown that the overall polarity and packing of the distal residues are key factors in regulating the rate and equilibrium constants for ligand bindings.[13]

In addition to mutagenic analyses of heme binding sites on proteins, the value of using synthetic iron porphyrins as Hb and Mb active-site models has also been amply demonstrated.[14,15] Tetrakis(α,α,α,α-*o*-pivalamido)phenylporphinato-iron(II) "picket-fence porphyrin" of Collman et al.[16] was a pioneering molecule, which forms an O_2 adduct complex at room temperature that is quite stable and shows a high O_2 binding affinity. The polar secondary amide groups in the four fences were believed to contribute to the high O_2 affinity. Moementeau and Lavalette[17] first demonstrated the distal polarity effect on the O_2 binding to the "hanging-base porphyrins". The presence of the amide groups in the strapped handle over the porphyrin macrocycle yielded a 9-fold higher O_2 binding affinity compared to the ether-bond analogue; it was due to an 8-fold reduction in the dissociation rate constant. This polarity effect of the substituent

(10) Monzani, E.; Bonafè, B.; Fallarini, A.; Redaelli, C.; Casella, L.; Minchiotti, L.; Galliano, M. *Biochim. Biophys. Acta.* **2001**, *1547*, 302−312.
(11) (a) Komatsu, T.; Ohmichi, N.; Zunszain, P. A.; Curry, S.; Tsuchida, E. *J. Am. Chem. Soc.* **2004**, *126*, 14304−14305. (b) Komatsu, T.; Ohmichi, N.; Nakagawa, A.; Zunszain, P. A.; Curry, S.; Tsuchida, E. *J. Am. Chem. Soc.* **2005**, *127*, 15933−15942.
(12) Phillips, S. E. V.; Schoenborn, B. P. *Nature* **1981**, *292*, 81−82.
(13) (a) Olson, J. S.; Mathews, A. J.; Rohlfs, R. J.; Springer, B. A.; Egeberg, K. D.; Sligar, S. G.; Tame, J.; Renaud, J.-P.; Nagai, K. *Nature* **1988**, *336*, 265−266. (b) Rohlfs, R.; Mathews, A. J.; Carver, T. E.; Olson, J. S.; Springer, B. A.; Egeberg, K. D.; Sligar, S. G. *J. Biol. Chem.* **1990**, *265*, 3168−3176. (c) Springer B. A.; Sligar, S. G.; Olson, J. S.; Phillips, G. N., Jr. *Chem. Rev.* **1994**, *94*, 699−714.
(14) Momenteau, M.; Reed, C. A. *Chem. Rev.* **1994**, *94*, 659−698.
(15) Collman, J. P.; Fu, L. *Acc. Chem. Res.* **1999**, *32*, 455−463.
(16) (a) Collman, J. P.; Gagne, R. R.; Halbert, T. R.; Marchou, J.-C.; Reed. C. A. *J. Am. Chem. Soc.* **1973**, *95*, 7869−7870. (b) Collman, J. P.; Gagne, R. R.; Reed, C. A.; Halbert, T. R.; Lang, G.; Robinson, W. T. *J. Am. Chem. Soc.* **1975**, *97*, 1427−1439. (c) Collman, J. P.; Brauman, J. I.; Iverson, B. L.; Sessler, J. L.; Morris, R. M.; Gibson, Q. H. *J. Am. Chem. Soc.* **1983**, *105*, 3052−3064.
(17) Momenteau, M.; Lavalette, D. *J. Chem. Soc., Chem. Commun.* **1982**, 341−343.

was also well illustrated by our "double-sided porphyrins" having ester fences with a 23-fold lower O_2 binding affinity relative to the picket-fence porphyrin.[18]

In view of these investigations, we reasoned that systematic variation of the steric hindrance and local polarity of the heme pocket in subdomain IB of HSA would allow us to modulate the O_2 binding affinity of rHSA−heme. In this study, we designed and generated nine rHSA(triple mutant)−heme complexes, in which the specific third mutation was introduced into three different positions near the O_2 binding site. The effects of the engineered distal amino acids on the O_2 and CO binding properties of the prosthetic heme group have been physicochemically and kinetically characterized. We now present a new chemistry of albumin-based artificial hemoproteins that would serve as an entirely synthetic O_2 carrier with a controllable ligand binding affinity.

Experimental Section

Materials and Apparatus. All materials were reagent-grade and were used as purchased without further purification. Iron(III) protoporphyrin IX (hemin) chloride was purchased from Fluka. UV−vis absorption spectra were obtained on an Agilent 8453 UV−visible spectrophotometer equipped with an Agilent 89090A temperature control unit. Kinetic measurements for the O_2 and CO bindings were carried out on a Unisoku TSP-1000WK time-resolved spectrophotometer with a Spectron Laser Systems SL803G-10 Q-switched Nd:YAG laser, which generated a second-harmonic (532 nm) pulse of 6-ns duration (10 Hz).[11b] A 150 W xenon arc lamp was used as the probe light source. The gas mixture with the desired partial pressure of O_2/CO/N_2 was prepared by a Kofloc Gasblender GB-3C. MCD spectra were measured by a Jasco J-820 circular dichrometer.

Preparations of rHSA Triple Mutants and Their Heme Complexes. The designed rHSA triple mutants were prepared according to our previously reported techniques.[11] The third mutation (L185N, L185Q, L185H, L182H, R186H, R186L, or R186F) was introduced into the HSA coding region in a plasmid vector encoding the double mutants [rHSA(I142H/Y161F) [rHSA(HF)] or rHSA(I142H/Y161L) [rHSA(HL)]][11] by use of the Stratagene QuikChange mutagenesis kit. All mutations were confirmed by DNA sequencing. The plasmid was then digested by *Not*I and introduced into yeast (*Pichia pastoris* GS115) by electroporation. The expression protocols and media formulations were as previously described.[11b] Briefly, the clones were grown in BMGY medium and transferred to BMMY medium for induction with methanol in baffled shaking flasks at 30 °C, 200 rpm. The obtained proteins were harvested from the growth medium by precipitation with ammonium sulfate and purified by a Cibacron Blue column of Blue Sepharose 6 Fast Flow (Amersham Pharmacia Biotech). The rHSA triple mutants were finally subjected to gel filtration on an ÄKTA Prime Plus FPLC system with a Superdex 75 preparative-grade column (Amersham Pharmacia Biotech). The protein concentration was assayed by measuring the absorbance at 280 nm ($\epsilon_{280} = 3.4 \times 10^4\ M^{-1}\ cm^{-1}$) and by SDS−PAGE.

The ferric rHSA(mutant)−hemin complexes [hemin:rHSA(mutant) molar ratio of 1:1] were prepared by established procedures.[9,11] The resulting samples were analyzed by SDS−PAGE to confirm a pure preparation. The 50 mM phosphate buffered solution (pH 7.0, 3 mL) of rHSA(mutant)−hemin ([hemin] = 10 μM) in a 10-mm path length optical quartz cuvette sealed with a rubber septum was purged with Ar for 40 min. A small excess amount of degassed aqueous sodium dithionate was added by a microsyringe to the sample under an Ar atmosphere to reduce the central ferric ion of the hemin, to give the ferrous rHSA(mutant)−heme complexes.

O_2 and CO Binding Parameters. The O_2 or CO recombination with the heme after nanosecond laser flash photolysis of hemeO_2 or hemeCO occurs according to eq 1 with the association rate constant (k_{on}^L) and dissociation rate constant (k_{off}^L):[11,16c,19]

$$\text{hemeL} \xrightarrow{h\nu} \text{heme} \underset{k_{off}^L}{\overset{k_{on}^L}{\rightleftharpoons}} \text{hemeL} \qquad (1)$$

where L = O_2 or CO. The CO association rate (k_{on}^{CO}) was simply measured by following the absorption at 425 nm after laser pulse irradiation to rHSA(mutant)−hemeCO at 22 °C.[11] The O_2 association rate constant ($k_{on}^{O_2}$) and O_2 binding equilibrium constant K^{O_2} [= $(P_{1/2}^{O_2})^{-1}$] can be determined by a competitive rebinding technique by use of gas mixtures with different partial pressures of O_2/CO/N_2 at 22 °C.[11,16c,19] The relaxation curves that accompanied the O_2 or CO recombination were analyzed by single- or double-exponential profiles with Unisoku Spectroscopy & Kinetics software. The O_2 dissociation rate ($k_{off}^{O_2}$) was calculated from $k_{on}^{O_2}/K^{O_2}$.

The CO dissociation rate constant (k_{off}^{CO}) was measured by displacement with NO for rHSA(mutant)−hemeCO at 22 °C.[11b] The time course of the UV−vis absorption change that accompanied the CO dissociation was fitted to two single exponentials. The CO binding constants [$K^{CO} = (P_{1/2}^{CO})^{-1}$] were calculated from k_{on}^{CO}/k_{off}^{CO}. Fresh solutions of rHSA(mutant)−heme were normally made up for each set of experiments.

Magnetic Circular Dichroism Spectroscopy. MCD for the 50 mM potassium phosphate buffered solutions (pH 7.0) of rHSA(mutant)−hemin or −heme complex (10 μM) were measured under Ar and CO atmospheres with a 1.5 or 1.65 T electromagnet at 22 °C.

Results and Discussion

Design of Distal Pocket with Asn, Gln, and His. We recently compared the O_2 and CO binding properties of the rHSA(double mutant)−heme complexes [rHSA(HF)−heme and rHSA(HL)−heme] and found evidence for a noteworthy distal-side steric effect on ligand binding.[11b] The rHSA(HF)−heme complex binds O_2 and CO about 4−6 times more tightly than rHSA(HL)−heme, primarily because of enhanced association rate constants. Structurally, this affect appears to be due to the concerted effects of the residues at positions 161 and 185 on ligand binding. In the rHSA(HF)−heme complex, the bulky aromatic side chain of Phe-161 is presumed to prevent rotation of the neighboring Leu-185, thereby providing easy access to the O_2 binding site in the distal pocket (Figure 2a). In contrast, the substitution of Phe-161 by the smaller Leu-161 may allow rotation of the isopropyl group of Leu-185, which reduces the volume of the distal side (Figure 2b) and hinders association of O_2 and CO ligands with the heme iron atom. On the basis of these findings, we reasoned that other modifications of the heme pocket architecture would allow us to further modulate its O_2 binding properties.

One approach to enhancing the O_2 binding affinities of rHSA(HF)−heme and rHSA(HL)−heme would be to introduce a histidine into an appropriate position on the distal side of the heme. The N_ϵ atom of His may act as a proton donor to form an H-bond with the coordinated O_2. However, another important requirement in this molecular design is to prevent the formation

(18) (a) Komatsu, T.; Hasegawa, E.; Nishide, H.; Tsuchida, E. *J. Chem. Soc., Chem. Commun.* **1990**, 66−68. (b) Tsuchida, E.; Komatsu, T.; Arai, K.; Nishide, H. *J. Chem. Soc., Dalton Trans.* **1993**, 2465−2469.

(19) Traylor, T. G.; Tsuchiya, S.; Campbell, D.; Mitchel, M.; Stynes, D.; Koga, N. *J. Am. Chem. Soc.* **1985**, *107*, 604−614.

(20) The pictures were produced on the basis of crystal structure coordinatex of rHSA(wt)−hemin (1O9X, ref 9) by use of PyMOL: DeLano, W. L. The PyMOL Molecular Graphics System; DeLano Scientific: San Carlos, CA, 2002.

of a six-coordinate low-spin ferrous complex. The bis-histidyl hemochromes are normally autoxidized by O_2 via an outer-sphere mechanism as well as by inner-sphere pathways involving the metal-coordinated O_2.[21−23] The distal amino acid must therefore be located relatively far (>4 Å) from the central iron.

Our modeling experiments suggested that the favorable position for the distal His insertion was Leu-185, which is in the final helix in subdomain IB and forms part of the top of the distal pocket (Figure 1). Leu-182 and Arg-186 were also considered likely to be good candidate positions for the introduction of an amide-containing side chain designed to stabilize O_2 binding (see below). In elegant studies on Mb, Rohlfs and co-workers showed that Gln, which has a primary amide group potential to form an H-bond, was able to substitute effectively for the stabilizing role of the distal histidine (His-64).[13b,c] Thus, we decided to vary the polarity of the distal side of the heme in rHSA(HF) and rHSA(HL) by replacing Leu-185 with Asn, Gln, and His by site-directed mutagenesis. The Asn residue should behave similarly to Gln, although a rMb-(H64N) mutant has never been reported. The His-185 mutation was only done for rHSA(HF), because His-185 could be long enough to bind to the sixth coordinate position of the heme if allowed the greater freedom of movement that would occur in the rHSA(HL) background. As a result, five triple mutants [rHSA(HF/L185N), rHSA(HL/L185N), rHSA(HF/L185Q), rHSA-(HL/L185Q), and rHSA(HF/L185H)] were cloned and their hemin complexes were prepared.

Ferric States of L185N, L185Q, and L185H Mutants. The site-specific mutations with Asn, Gln, and His were successfully introduced into the Leu-185 position of rHSA(HF) or rHSA-(HL), and the proteins were purified to homogeneity as determined by SDS−PAGE. The rHSA(mutant)−hemin complexes produced from these proteins were stable for several months at 4 °C without precipitation.

The UV−vis absorption spectra of the five rHSA(triple mutant)−hemin complexes are essentially the same regarding their general features (Figure 3, Table 1). When analyzed by MCD spectroscopy to evaluate the redox state, spin state, and axial ligand environment, all the ferric rHSA(triple mutant)−hemins showed a characteristic MCD with similar S-shaped patterns in the Soret band region, though their intensities were dependent on the nature of the distal amino acid (Figure 4). Vickery et al.[24] previously reported that the Soret MCD intensity of the ferric Mb with different anions at the sixth coordinate position was correlated with the amount of low-spin component. rHSA(HL)−hemin showed almost the same band as ferric Mb, in which one water axially coordinates to the sixth position of the hemin to produce the aquo complex.[11,24,25] In contrast, rHSA-(HF/L185H)−hemin showed 3-fold greater intensity at 405 nm. This is probably caused by the coexistence of a low-spin six-coordinate hemin. Introduction of Asn or Gln at position 185

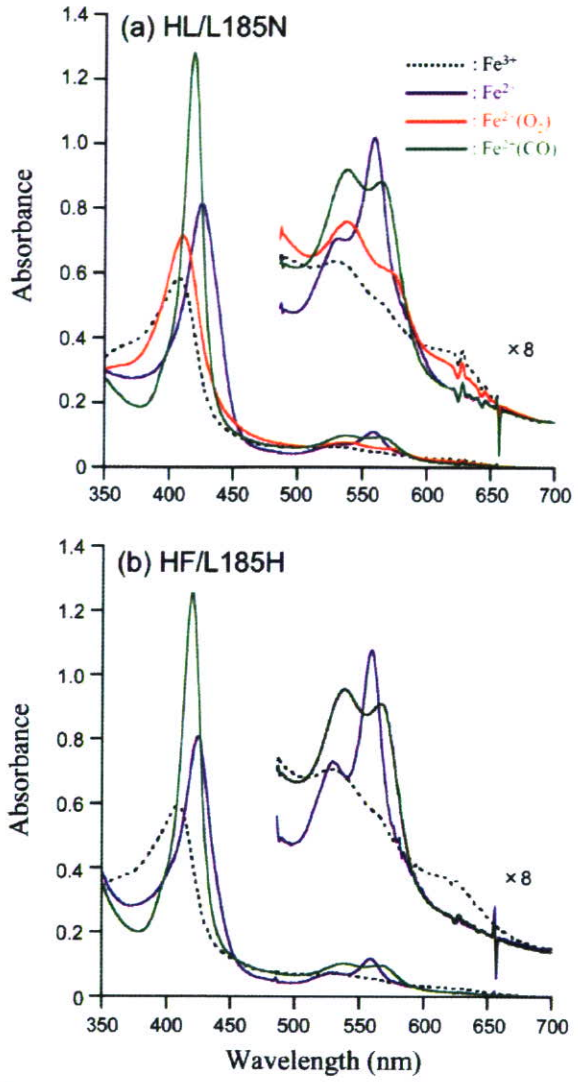

Figure 3. UV−vis absorption spectral changes of (a) rHSA(HL/L185N)−heme and (b) rHSA(HF/L185H)−heme complexes in 50 mM potassium phosphate buffered solution (pH 7.0, 22 °C).

gave intermediate effects, though mutants with Q185 yielding a slightly more intense peak at 405 nm. Overall, our MCD results for these five rHSA(triple mutant)−hemin complexes imply that the introduction of the distal nitrogenous residue at the 185 position tends to increase the ferric low-spin nature.

Ferrous States of L185N, L185Q, and L185H Mutants and O_2 Binding. rHSA(triple mutant)−hemins were easily reduced to form the ferrous complexes by adding a small excess of aqueous sodium dithionate under an Ar atmosphere. rHSA(HF/L185N)−heme, rHSA(HL/L185N)−heme, and rHSA(HL/L185Q)−heme each showed a visible absorption band at 558−559 nm with a small shoulder at 530 nm (Figure 3a; Figure S1, Supporting Information), that was similar to the spectra observed for rHSA(HF)−heme, rHSA(HL)−heme,[11b] deoxyMb,[27] and synthetic chelated protoheme.[26] The spectral patterns clearly indicated the formation of a five-N-coordinate high-spin complex. In contrast, in the spectra of rHSA(HF/L185Q)−heme and

(21) Chu, M. M. L.; Castro, C. E.; Hathaway, G. M. *Biochemistry* **1978**, *17*, 481−486.
(22) Tsuchida, E.; Nishide, H.; Sato, Y.; Kaneda, M. *Bull. Chem. Soc. Jpn.* **1982**, *55*, 1890−1895.
(23) Uno, T.; Sakamoto, R.; Tomisugi, Y.; Ishikawa, Y.; Wilkinson, A. *Biochemistry* **2003**, *42*, 10191−10199.
(24) Vickery, L.; Nozawa, T.; Sauer, K. *J. Am. Chem. Soc.* **1976**, *98*, 343−350.
(25) Collman, J. P.; Basolo, F.; Bunnenberg, E.; Collins, T. J.; Dawson, J. H.; Ellis, P. E., Jr.; Marrocco, M. L.; Moscowitz, A.; Sessler, J. L.; Szymanski, T. *J. Am. Chem. Soc.* **1981**, *103*, 5636−5648.
(26) Traylor, T. G.; Chang, C. K.; Geibel, J.; Berzinis, A.; Mincey, T.; Cannon, J. *J. Am. Chem. Soc.* **1979**, *101*, 6716−6731.
(27) Antonini, E.; Brunori, M. *Hemoglobin and Myoglobin in Their Reactions with Ligands*; North-Holland: Amsterdam, 1971; p 18.

Table 1. UV−vis Absorption Spectral Data of rHSA(mutant)−Heme Complexes[a]

hemoproteins	λ_{max} (nm) Fe^{3+}	Fe^{2+}	$Fe^{2+}O_2$	$Fe^{2+}CO$
rHSA(HF)−heme[b]	402, 533, 620	425, 532(sh), 559	411, 538, 576	419, 538, 565
rHSA(HL)−heme[b]	402, 533, 620	426, 531(sh), 559	412, 537, 573	419, 538, 565
rHSA(HF/L185N)−heme	406, 528, 618	425, 530(sh), 559	411, 540, 575	419, 539, 566
rHSA(HL/L185N)−heme	407, 530, 620	425, 530(sh), 559	411, 537, 575	419, 537, 564
rHSA(HF/L185Q)−heme	406, 530, 620	424, 528, 558		419, 538, 566
rHSA(HL/L185Q)−heme	406, 530, 620	425, 530(sh), 558	411, 537, 574[c]	419, 537, 566
rHSA(HF/L185H)−heme	407, 528, 620	424, 528, 558		419, 538, 566
rHSA(HL/L182H)−heme	410, 532, 624	425, 530, 559		419, 539, 567
rHSA(HF/R186H)−heme	411, 533, 565	424, 529, 560		420, 539, 568
rHSA(HL/R186L)−heme	406, 530, 620	426, 531(sh), 559	411, 539, 576	419, 539, 567
rHSA(HL/R186F)−heme	405, 532, 621	426, 531(sh), 559	410, 535, 571	419, 538, 568
Mb[d]	409, 503, 548(sh), 632	434, 557	418, 544, 581	423, 541, 579
chelated heme[e]	408, 540, 565	427, 530, 558	414, 543, 575	420, 540, 569

[a] In 50 mM potassium phosphate buffered solution (pH 7.0) at 22 °C. [b] Reference 11b. [c] At 5 °C. [d] Horse muscle myoglobin (Sigma); ref 11b. [e] In DMF/H_2O (7/3) at 15 °C; ref 26.

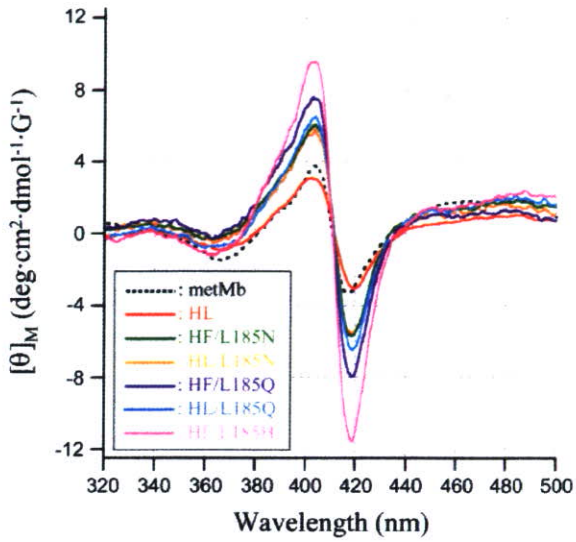

Figure 4. MCD spectra of rHSA(185-mutant)−hemin complexes in 50 mM potassium phosphate buffered solution (pH 7.0, 22 °C).

rHSA(HF/L185H)−heme, the β band at 528 nm appeared relatively sharp (Figure 3b), which suggests partial formation of a six-coordinate heme complex. This is consistent with the finding that the ferric state of these two mutant complexes had the highest peaks in the MCD.

The Soret MCD spectra of ferrous rHSA(HF/L185N)−heme, rHSA(HL/L185N)−heme, and rHSA(HL/L185Q)−heme under Ar atmosphere are dominated by an intense positive peak at 433 nm and a small trough at 402 nm as expected for the Faraday *C*-terms for high-spin ferrous porphyrins like deoxyMb (Figure 5a).[24,25] In contrast to these three mutant complexes, rHSA(HF/L185Q)−heme and rHSA(HF/L185H)−heme show weaker intensity in the Soret band region and greater intensity in the visible region (Figure 5b).

On the basis of all the UV−vis absorption and MCD spectral results, we concluded that the reduced ferrous heme is axially coordinated by His-142 at the core of the heme pocket in rHSA-(mutant) and forms a five-N-coordinate high-spin ferrous complex under an Ar atmosphere in the case of HF/L185N, HL/L185N, and HL/L185Q mutants (Figure 6a,b,d). In addition to the His-142 ligation, Gln-185 and His-185 partially interact with the sixth coordinate position of the central Fe^{2+} ion of the

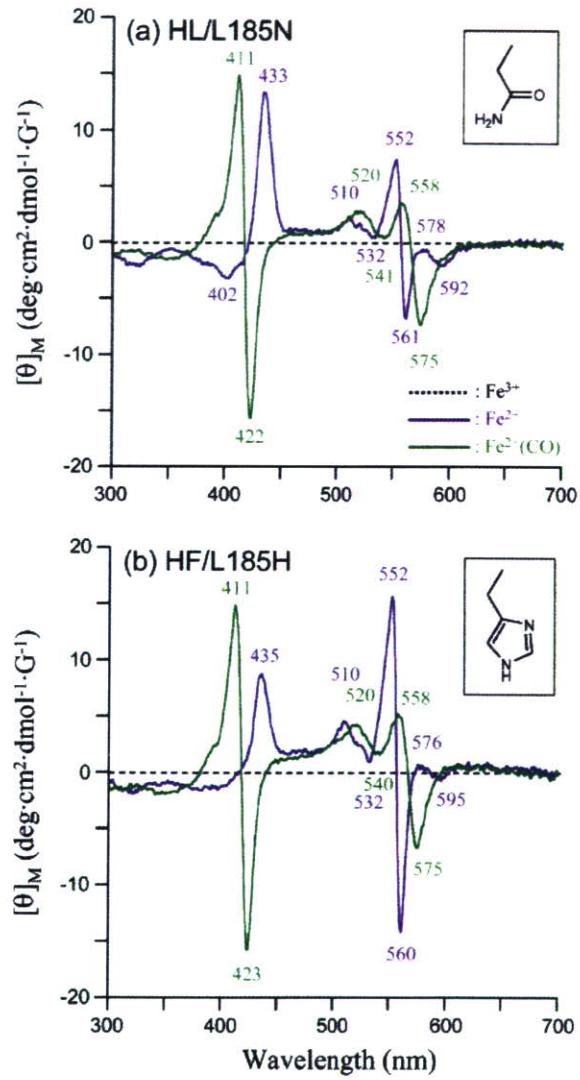

Figure 5. MCD spectral changes of (a) rHSA(HL/L185N)−heme and (b) rHSA(HF/L185H)−heme complexes in 50 mM potassium phosphate buffered solution (pH 7.0, 22 °C).

heme in the HF/L185Q and HF/L185H mutants in spite of the bulky aromatic ring of Phe-161 (Figure 6c,e). We postulated that rHSA(HL/L185Q)−heme would also form a six-coordinate

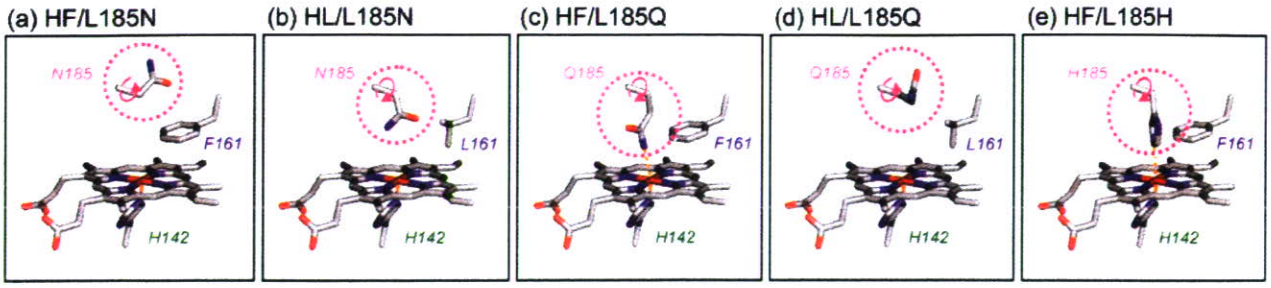

Figure 6. Structural models of the heme pocket in rHSA(triple mutant)−heme complexes: distal-side effects of engineered amino acids at position 185.

low-spin complex, because the small Leu-161 should allow additional room for rotation of Gln-185. However, it yielded a five-coordinate high-spin ferrous complex (Figure S1). This suggests that the flexible Gln-185 may interact with neighboring amino acids (Figure 6d) and underscores the difficulty in accurately predicting the impact of amino acid substitutions.

Upon exposure of the rHSA(HF/L185N)−heme and rHSA-(HL/L185N)−heme solutions to O_2, the UV−vis absorptions immediately changed to that of the O_2 adduct complex at 22 °C (Figure 3a, Table 1).[11,26,27] However, the rHSA(HL/L185Q)−heme complex bound O_2 only at 5 °C (Figure S1a) and was observed to autoxidize rapidly at 22 °C. This rapid oxidation may suggest that the distal side of the heme has an open structure, which allows easy access of water to the heme, thereby facilitating autoxidation.[28] The rHSA(HF/L185Q)−heme and rHSA(HF/L185H)−heme complexes, both of which exhibit side-chain interactions with the sixth coordinate position of the heme, were immediately oxidized by O_2 even at low temperature (5 °C).

After introduction of CO gas, all the hemoproteins produced stable carbonyl complexes with identical absorption spectral patterns (Figures 3 and S1a, Table 1).[11,26,27] In every case the carbonyl rHSA(triple mutant)−heme complexes exhibited the same S-shaped MCDs, which correspond to the *A*-term bands for the diamagnetic low-spin protoheme with CO and axial His coordinations (Figures 5 and S1b).[24,25] This result implies that in the carbonyl complexes the Asn-185 and Gln-185 residues do not act as a proximal base instead of His-142.

O_2 and CO Binding Parameters of L185N Mutants. By use of laser flash photolysis, analysis of the kinetics of ligand binding to the double mutants rHSA(HF)−heme and rHSA-(HL)−heme revealed that the asymmetric iron protoporphyrin IX molecule is accommodated in subdomain IB in two different orientations (180° rotational isomers).[11] As a result, there exist two geometries of the axial His-142 coordination to the central Fe^{2+} ion of the heme (species I and II). In species I, the proximal His coordinates to the heme without strain, while in species II, the ligation involves some distortion, resulting in weaker O_2 binding. The bending strain in the proximal His−Fe^{2+} bond in species II increases the dissociation rate constant and decreases the association rate for CO, whereas it increases the O_2 dissociation rate without changing the kinetics of the O_2 association.[16c,19] Consequently, the entire absorption decay accompanying the CO recombination with rHSA(HF)−heme or rHSA(HL)−heme was composed of two single exponentials, but the rebinding process of O_2 followed a simple monophasic decay. In rHSA(triple mutant)−hemes, this alternative geometry of the heme plane would also arise in the same manner.

We again used laser flash photolysis to characterize the O_2 and CO binding properties of the rHSA(triple mutant)−heme complexes. As expected, the binding behavior of O_2 for rHSA-(HF/L185N)−heme and rHSA(HL/L185N)−heme was broadly similar to that of the double mutants. However, detailed analysis reveals that the absorption decay accompanied by O_2 rebinding to the heme was composed of two very similar phases (Figure S2, Supporting Information). Numerous investigations of the synthetic iron porphyrins have demonstrated that the "distal-side steric effect" is the only factor that influences the association rate constant for O_2.[16c,19] The double-exponential profiles for O_2 association are therefore likely to indicate that there are two distinct conformations of the distal Asn-185 above the heme. The amplitude ratio of the two phases was approximately 1:1 for rHSA(HL/L185N)−heme, suggesting that half of the Asn residue may turn toward the inside of the heme pocket and the other turns to the outside (Figure 6b). These two conformers of the distal Asn-185 residue also influence the association rate for CO. If we were to take this minimal effect into account, the CO rebinding process would have to be analyzed as four phases. However, (i) it would be too complicated to comprehend the fundamental aspects of the ligand binding properties of rHSA(triple mutant)−heme, and (ii) the observed distal-side effect is less significant compared to the major proximal-side steric effect in this system. Hence, the absorbance decays after laser pulse irradiation to rHSA(HF/L185N)−hemeCO and rHSA(HL/L185N)−hemeCO were fitted by biphasic kinetics. The ratio of the amplitude of the dominant fast phase (species I) and minor slow phase (species II) was approximately 7:3 for rHSA(HF/L185N)−heme and 3:2 for rHSA(HL/L185N)−heme. These values were within the same range observed in the rHSA(double mutant)−heme complexes.[11] Concomitantly, the O_2 association rate of rHSA(HF/L185N)−heme or rHSA(HL/L185N)−heme was determined as one value by weighted averaging of the $k_{on}^{O_2}$ values for the two phases (Table 2).

In general, k_{off}^{CO} is a simple indicator of the bending strain in the proximal His coordination to the central Fe^{2+} ion.[16c,19] rHSA(HF)−heme, rHSA(HL)−heme, rHSA(HF/L185N)−heme, and rHSA(HL/L185N)−heme exhibited similar k_{off}^{CO} values in species I (0.008−0.013 s^{-1}) and they are identical to that of Hb(α) (R-state) (0.009 s^{-1}) (Table 3).[29] This result indicated that the axial His-142 ligation to the heme in these artificial hemoproteins has the same features as that of Hb.

(28) Brantley, R. E., Jr.; Smerdon, S. J.; Wilkinson, A. J.; Singleton, E. W.; Olson, J. S. *J. Biol. Chem.* **1993**, *268*, 6995−7010.

(29) Sharma, V. S.; Schmidt, M. R.; Ranney, H. M. *J. Biol. Chem.* **1976**, *251*, 4267−4272.

Table 2. O_2 Binding Parameters of rHSA(mutant)−Heme Complexes[a]

hemoproteins	$k_{on}^{O_2}$ (μM^{-1} s^{-1})	$k_{off}^{O_2}$ (ms^{-1}) I	$k_{off}^{O_2}$ (ms^{-1}) II	$P_{1/2}^{O_2}$ (Torr) I	$P_{1/2}^{O_2}$ (Torr) II
rHSA(HF)−heme[b]	20	0.10	0.99	3	31
rHSA(HL)−heme[b]	7.5	0.22	1.70	18	134
rHSA(HF/L185N)−heme	26	0.10	1.03	2	24
rHSA(HL/L185N)−heme	14	0.02	0.29	1	14
rHSA(HL/R186L)−heme	25	0.41	8.59	10	209
rHSA(HL/R186F)−heme	21	0.29	7.01	9	203
Hb(α) (R-state)[c]	33[d]	0.013[e]		0.24	
Mb[f]	14	0.012		0.51	
RBC[g]				8	

[a] In 50 mM potassium phosphate buffered solution (pH 7.0) at 22 °C. I or II indicates species I or II. [b] Reference 11. [c] Human hemoglobin α-subunit. [d] In 0.1 M phosphate buffer (pH 7.0, 21.5 °C); ref 30. [e] In 10 mM phosphate buffer (pH 7.0, 20 °C); ref 31. [f] Sperm whale myoglobin, in 0.1 M potassium phosphate buffer (pH 7.0, 20 °C); ref 13b. [g] Human red cell suspension, in isotonic buffer (pH 7.4, 20 °C); ref 32.

Table 3. CO Binding Parameters of rHSA(mutant)−Heme Complexes[a]

hemoproteins	k_{on}^{CO} (μM^{-1} s^{-1}) I	k_{on}^{CO} (μM^{-1} s^{-1}) II	k_{off}^{CO} (s^{-1}) I	k_{off}^{CO} (s^{-1}) II	$P_{1/2}^{CO}$ (Torr) I	$P_{1/2}^{CO}$ (Torr) II
rHSA(HF)−heme[b]	6.8	0.72	0.009	0.061	0.0011	0.068
rHSA(HL)−heme[b]	2.0	0.27	0.013	0.079	0.0053	0.240
rHSA(HF/L185N)−heme	7.7	1.09	0.008	0.043	0.0008	0.032
rHSA(HL/L185N)−heme	6.8	1.60	0.008	0.039	0.0010	0.020
rHSA(HL/R186L)−heme	5.0	0.57	0.011	0.165	0.0018	0.234
rHSA(HL/R186F)−heme	7.9	1.12	0.010	0.148	0.0010	0.107
Hb(α) (R-state)[c]	4.6[d]		0.009[e]		0.0016[f]	
Mb[g]	0.51		0.019		0.030	

[a] In 50 mM potassium phosphate buffered solution (pH 7.0) at 22 °C. I or II indicates species I or II. [b] Reference 11. [c] Human hemoglobin α-subunit. [d] In 50 mM potassium phosphate buffer (pH 7.0, 20 °C); ref 33. [e] In 0.1 M phosphate buffer (pH 7.0, 20 °C); ref 29. [f] Calculated from $(k_{on}^{CO}/k_{off}^{CO})^{-1}$. [g] Sperm whale myoglobin, in 0.1 M potassium phosphate buffer (pH 7.0, 20 °C); ref 13b.

Effect of Asn-185 Residue on O_2 Binding Affinity. The O_2 and CO binding parameters for the rHSA(HF)−heme and rHSA(HF/L185N)−heme complexes did not show any significant differences. The bulky benzyl side chain of Phe-161 may retard rotation of the polar amide group of Asn-185 and thereby maintain the polarity and size of the distal pocket (Figure 6a). In contrast, there are marked differences in the comparison of the O_2 and CO binding parameters for rHSA(HL)−heme and rHSA(HL/L185N)−heme. First, the presence of Asn rather than Leu at position 185 resulted in 2- and 3−6-fold increases in the association rate constants for O_2 and CO, respectively. As described above, the kinetics of O_2 binding to rHSA(HL/L185N)−heme actually consist of two phases. The Asn may partly rotate upward, which provides a somewhat greater space for the distal pocket. This presumably increases the association rate constants. Second, Asn-185 induced 18- and 10-fold increases in the O_2 binding affinity for species I and II, respectively (Table 2); these increases were predominantly due to the 6−11-fold diminution of the $k_{off}^{O_2}$ values. This corresponds to a free energy difference of −1.8 kcal mol^{-1} at 22 °C that may be attributable to a H-bond interaction with the bound O_2. This is consistent with the observation that, in HbO_2 and MbO_2, the distal His-64 stabilizes the coordinated O_2 by −0.6∼−1.4 kcal mol^{-1} due to the H-bonding.[13] Unfortunately, attempts to measure the stretching frequency of the bound O_2 molecule in rHSA(HL/L185N)−heme by infrared spectroscopy failed because the O_2 adduct complex was not sufficiently stable. Nevertheless, it is noteworthy that the high O_2 binding affinity ($P_{1/2}^{O_2}$ 1 Torr) for rHSA(HL/L185N)−heme is now close to that of natural Hb(α) (0.24 Torr)[30,31] and Mb (0.5 Torr)[13] (Table 2).

Replacement of L182 or R186 by His. Leu-182 and Arg-186 were also considered to be good candidates for introduction of the distal His, so we prepared the rHSA(HL/L182H) and rHSA(HF/R186H) triple mutants (Figure 1). Modeling trials demonstrated that neither of these introduced histidines is coplanar with the Fe−O−O moiety. Rather, they are positioned off to the side, so that there may be an oblique interaction with the coordinated O_2 and the heme center.

The rHSA(HL/L182H)−hemin complex and its reduced form showed spectra similar to those of rHSA(HF/L185H)−heme. In contrast, the color of the ferric rHSA(HF/R186H)−hemin solution was bright red, and the UV−vis absorption spectrum clearly showed the formation of a bis-histidine-coordinated low-spin ferric complex (Figure 7a).[22,26] The MCD intensity of the S-shaped curve in the Soret band region (Figure 8) was higher than that observed with rHSA(HF/L185H)−hemin (Figure 4). The chemical reduction of the Fe^{3+} complex results in very sharp β, α bands in the visible absorption spectrum (529, 560 nm) (Figure 7a). In MCD, we observed the loss of the strong *C*-terms in the Soret band and the appearance of intense *A*-terms corresponding to the α band (Figure 7b). They all resembled those of the typical bis-histidyl hemochrome, for example, cytochrome b_5,[34] soluble guanylcyclase,[35a] and bis-imidazole-bound protoheme,[22,26,35b] as well as Hpx.[1b] It can be concluded that rHSA(HF/R186H)−heme produced a strong six-coordinate low-spin ferrous complex under an Ar atmosphere. Unfortunately, the ferrous forms of both rHSA(HF/R186H)−heme and rHSA(HL/L182H)−heme were readily autoxidized upon the addition of O_2 gas. It is known that bis-histidyl hemochromes are rapidly oxidized by O_2 via an outer-sphere mechanism.[21] We have demonstrated that this also applies to our artificial hemoprotein, the rHSA(mutant)−heme system.

O_2 and CO Binding Parameters for R186L and R186F Mutants. We have clearly shown that the O_2 binding equilibrium and kinetics of rHSA−heme complexes may be significantly enhanced by site-directed mutagenesis. In fact, the O_2 binding affinity of the rHSA(HL/L185N)−heme complex (1 Torr) was shown to be similar to those of Mb and the high-affinity R-state of Hb(α). However, for saline solutions of artificial rHSA−heme complexes to provide effective lung-to-tissue O_2 transport in vivo, the affinity should be reduced to render it more similar to the affinity of human RBC ($P_{1/2}^{O_2}$ 8 Torr).[32] This requires an O_2 binding affinity that is intermediate between the values observed for rHSA(HL)−heme and rHSA(HL/L185N)−heme.

Both site-directed mutagenesis and synthetic porphyrin approaches have previously shown that an effective way to diminish the O_2 binding affinity of the heme is to introduce a

(30) Gibson, Q. H. *J. Biol. Chem.* **1970**, *245*, 3285−3288.
(31) Olson, J. S.; Andersen, M. E.; Gibson, Q. H. *J. Biol. Chem.* **1971**, *246*, 5919−5923.
(32) Imai, K.; Morimoto, H.; Kotani, M.; Watari, H.; Hirata, W.; Kuroda, M. *Biochim. Biphys. Acta.* **1970**, *200*, 189−197.
(33) Steinmeier, R. C.; Parkhurst, L. J. *Biochemistry* **1975**, *14*, 1564−1571.
(34) Vickery, L.; Salmon, A.; Sauer, K. *Biochim. Biophys. Acta.* **1975**, *386*, 87−98.
(35) (a) Burstyn, J. N.; Yu, A. E.; Dierks, E. A.; Hawkins, B. K.; Dawson, J. H. *Biochemistry* **1995**, *34*, 5896−5903. (b) Svastits, E. W.; Dawson, J. H. *Inorg. Chim. Acta.* **1986**, *123*, 83−86.

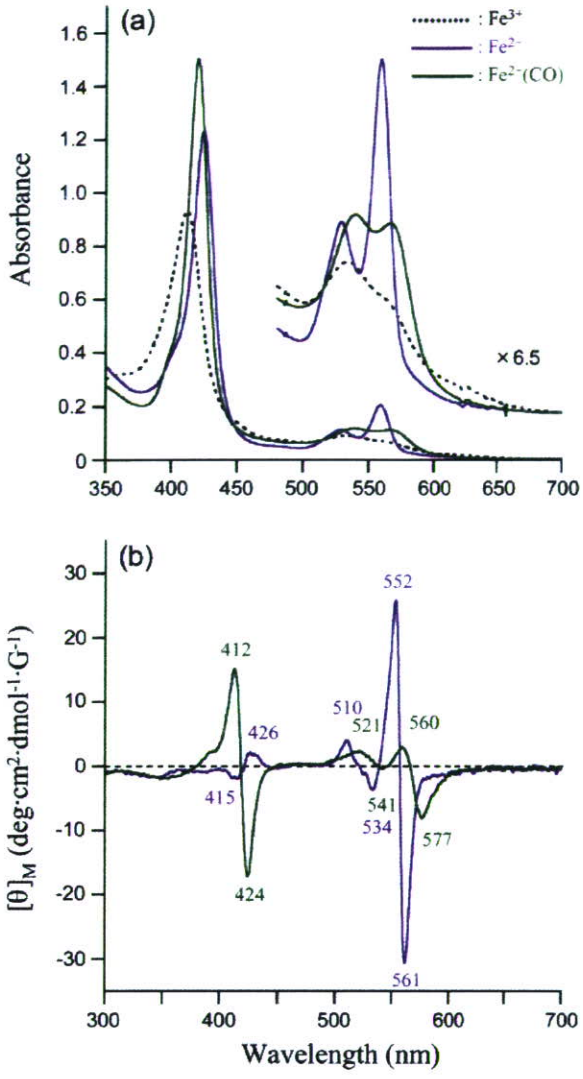

Figure 7. (a) UV−vis and (b) MCD spectral changes of rHSA(HF/R186H)−heme complex in 50 mM potassium phosphate buffered solution (pH 7.0, 22 °C).

hydrophobic amino acid (or substituent) around the O_2 binding site.[13,14,17−19] We expected that increasing the hydrophobicity of the distal side of the heme pocket by insertion of a nonpolar residue would reduce the O_2 binding affinity of the rHSA−heme complex. The most suitable position for this introduction could be at Arg-186, which is the entrance of the heme pocket and is rather close to the central Fe^{2+} ion.

Thus, we designed new triple mutants rHSA(HL/R186L) and rHSA(HL/R186F) in an effort to prepare rHSA-based artificial hemoproteins having the same O_2 binding affinity as human RBC (Figure 9). An important structural factor in these mutants is Y161L, which is likely to allow rotation of the isopropyl group of Leu-185 above the O_2 coordination site.

MCD spectra in the Soret band region of ferric rHSA(HL/R186L)−hemin and rHSA(HL/R186F)−hemin both showed very low intensity, essentially the same as that observed for rHSA(HL)−hemin (Figure 8). The reduced ferrous form demonstrated the characteristic UV−vis absorption and MCD spectra of the five-N-coordinate high-spin complex under an Ar atmosphere (Table 1; Figure S3, Supporting Information).

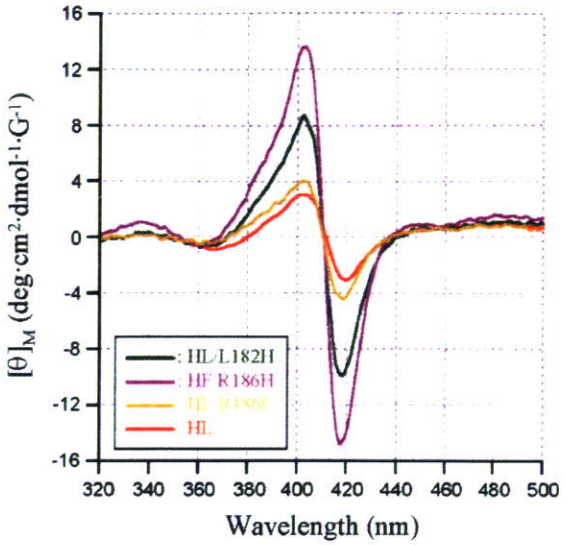

Figure 8. MCD spectra of rHSA(182-mutant)−hemin and rHSA(186-mutant)−hemin complexes in 50 mM potassium phosphate buffered solution (pH 7.0, 22 °C).

Upon bubbling of O_2 gas through the solutions, the spectral patterns were shifted to that of the O_2 adduct complex. The distinct features of all the spectra were quite similar to those of rHSA(HL)−heme.

Following laser flash photolysis, the absorption decays associated with O_2 recombination with rHSA(HL/R186L)−heme and rHSA(HL/R186F)−heme were monophasic, which suggests that the distal space in the pocket is uniform, in contrast to the L185N mutants. The kinetics for CO rebinding were still composed of double exponentials, consistent with the existence of two different geometries of the axial His-142 coordination to the central Fe^{2+} ion of the heme.

We previously showed that rHSA(HF) binds O_2 with significantly higher affinity than rHSA(HL) and reasoned that the presence of Leu rather than Phe at position 161 allowed a downward rotation of the adjacent L185 side chain that restricted access to the O_2 binding site on the heme group and reduced the affinity by a factor of 6 (Table 2).[11b] Strikingly, however, insertion of Leu or Phe at position 186 in the presence of Leu-161 [as in rHSA(HL/R186L)−heme and rHSA(HL/R186F)−heme complexes] yielded $k_{on}^{O_2}$ and k_{on}^{CO} values that were 3−4-fold higher than those of rHSA(HL)−heme. The presence of a hydrophobic residue at position 186 may restrict the mobility of Leu-185 and thereby enhance access to the O_2 binding site (Figure 9).

Overall, the O_2 and CO binding parameters of rHSA(HL/R186L)−heme and rHSA(HL/R186F)−heme were more similar to those of rHSA(HF)−heme. In species I, for example, the k_{off}^{CO} values were almost identical, which again implies unhindered axial coordination structures of His-142 to the heme; as a result, the CO binding affinities of these triple mutants ($P_{1/2}^{CO}$ 0.0010−0.0018 Torr) were close to that of the rHSA-(HF)−heme complex. In contrast, the O_2 dissociation rate constants of rHSA(HL/R186L)−heme and rHSA(HL/R186F)−heme were 3−4-fold higher than found for rHSA(HF)−heme, which modestly reduced the O_2 binding affinities (higher $P_{1/2}^{O_2}$). This could be due to the increase in the hydrophobicity in the distal pocket. Crucially, the O_2 binding affinities of rHSA(HL/

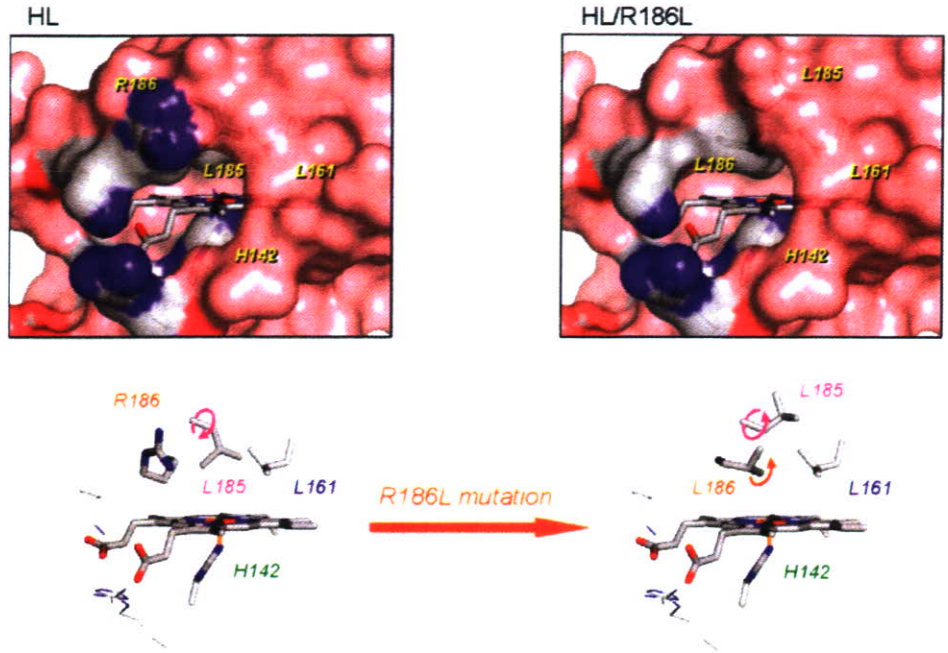

Figure 9. Structural models of rHSA(HL)−heme and rHSA(HL/R186L)−heme complexes. Introduction of R186L mutation may induce upward rotation of the L185 residue.

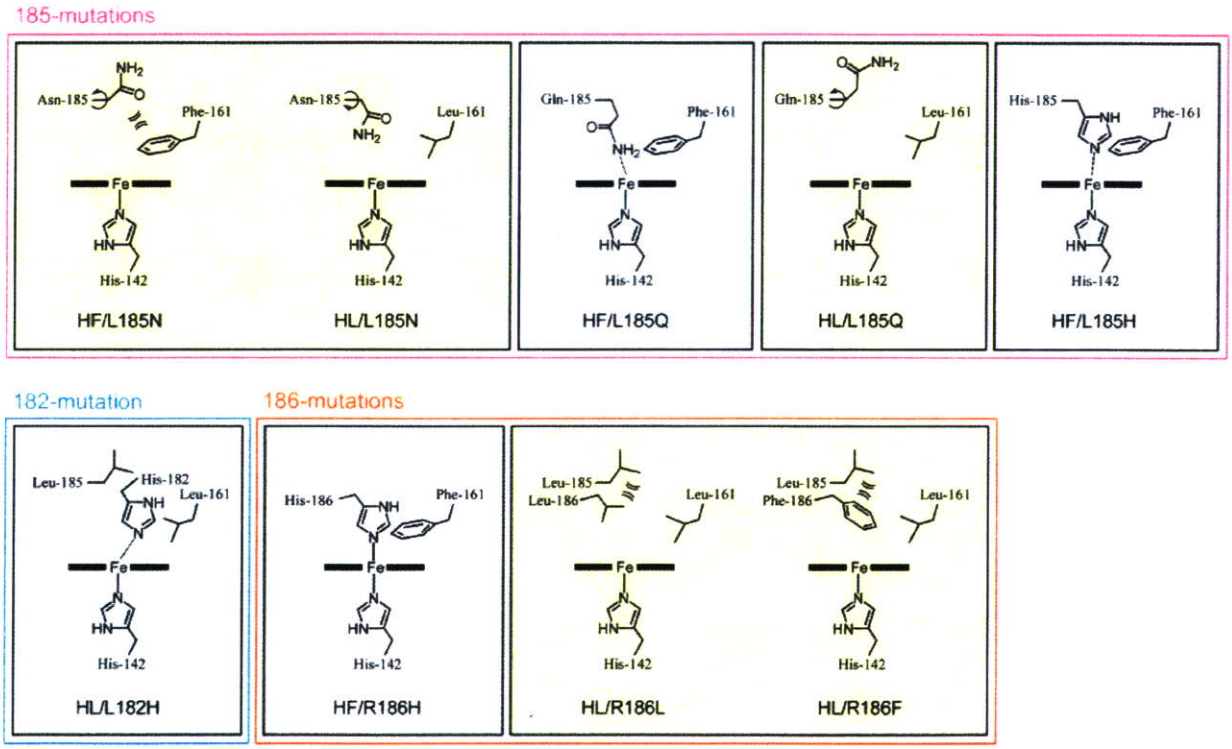

Figure 10. Schematic illustrations of the engineered distal amino acids in the heme pocket of rHSA(triple mutant)−heme: (yellow) five-coordinate high-spin ferrous complex; (blue) five-coordinate high-spin complex including six-coordinate low-spin ferrous complex; (pink) six-coordinate low-spin ferrous complex.

R186L)−heme ($P_{1/2}^{O_2}$ 10 Torr) and rHSA(HL/R186F)−heme ($P_{1/2}^{O_2}$ 9 Torr) are essentially indistinguishable from that of human RBC ($P_{1/2}^{O_2}$ 8 Torr). These results show that there are several different combinations of mutations that can confer the RBC-like O_2 binding affinity to the prosthetic heme group. Another possibility, yet to be explored, is that insertion of a proximal His into the 186 position would construct a distal pocket on the opposite side of the porphyrin plane (the Ile-142 side), that would provide somewhat different O_2 binding properties of the heme.